1   Similarities and differences of face and body perception in

2   the dog (*Canis familiaris*) and human brain

3   Magdalena Boch[1,2]*, Isabella C. Wagner[1], Sabrina Karl[3], Ludwig Huber[3+] and Claus

4   Lamm[1,4+]

5   [1]Social, Cognitive and Affective Neuroscience (SCAN) Unit, Department of Cognition, Emotion, and

6   Methods in Psychology, Faculty of Psychology, University of Vienna, Vienna, Austria

7   [2]Department of Cognitive Biology, Faculty of Life Sciences, University of Vienna, Vienna, Austria

8   [3]Comparative Cognition, Messerli Research Institute, University of Veterinary Medicine Vienna,

9   Medical University of Vienna and University of Vienna, Vienna, Austria

10   [4]Vienna Cognitive Science Hub, University of Vienna, Austria

11

12   [+]These authors share senior authorship.

13

14   *Corresponding author:

15   Email: magdalena.boch@univie.ac.at

16 **Abstract**

17   Accurately recognizing other individuals is fundamental for successful social

18   interactions. While the neural underpinnings of this skill have been studied

19   extensively in humans, less is known about the evolutionary origins of the brain areas

20   specialized for recognising faces or bodies. Studying dogs (*Canis familiaris*), a non-

21   primate species with the ability to perceive faces and bodies similarly to humans,

22   promises insights into how visuo-social perception has evolved in mammals. We

23   investigated the neural correlates of face and body perception in dogs (N = 15) and

24   humans (N = 40) using functional MRI. Combining uni- and multivariate analysis

25   approaches, we identified activation levels and patterns that suggested potentially

26   homologous occipito-temporal brain regions in both species responding to faces and

27   bodies compared to inanimate objects. Crucially, only human brain regions showed

28   activation differences between faces and bodies and partly responded more strongly

29   to humans compared to dogs. Moreover, only dogs represented both faces and dog

30   bodies in olfactory regions. Overall, our novel findings revealed a prominent role of

31   the occipito-temporal cortex in the perception of animate entities in dogs and humans

32   but suggest a divergent evolution of face and body perception. This may reflect

33   differences in the perceptual systems these species rely on to recognize others.

1   Introduction

34

35   The ability to detect and recognize another individual is a socio-cognitive skill

36   crucial for successful social interactions and survival. The face and body of another

37   human or non-human animal convey a wealth of social information beyond their

38   identity, such as when facilitating the correct categorization of another individual's

39   emotional state [1–7]. Consequently, accurate perception of faces and bodies is an

40   important building block for social perception.

41   Therefore, the neural underpinnings of face and body perception have been

42   studied extensively in humans. Decades of research revealed a predominant role of

43   the occipito-temporal cortex for the perception of others with distinct, but adjacent

44   regions specialized for face and body perception as part of the so-called ventral

45   visual pathway [8–17]. While the ventrolateral visual cortex responds to animate

46   compared to inanimate stimuli more generally [18–20], the sensitivity in the occipital

47   face and extrastriate body area (lateral occipital cortex), as well as the fusiform face

48   and fusiform body area (inferior temporal cortex) appear increased for faces or

49   bodies [10,11,24–28,12,13,15–17,21–23]. Regarding the recognition of another

50   individual's species-identity, previous research suggests a preference for human

51   faces compared to faces of other species (such as dogs or horses) [29,30],

52   potentially reflecting increased salience of conspecifics over heterospecifics.

53   The evolutionary history of the neural underpinnings of face and body

54   perception has been mainly investigated by comparative research in non-human

55   primates [23–27,31], and this has revealed a homologous visual pathway [e.g., 1 for

56   review]. However, apart from primate species, the neural bases of this socio-

57   cognitive ability and its potential origin in the mammalian brain remain largely

58   unstudied. Dogs' (*Canis familiaris*) ability to perceive and understand humans and

59   conspecifics has already been well-investigated using behavioural and eye-tracking

3

60   measures and yielded numerous comparable skills between dogs and humans. For

61   example, dogs can not only differentiate between faces [32,33], but even discriminate

62   facial emotional cues of humans and conspecifics [7,34,35]; and they demonstrate

63   complex behaviours such as visual perspective taking [36,37]. Thus, dogs constitute

64   an excellent model to study the evolution of visuo-social perception in mammals [38].

65   While first non-invasive canine neuroimaging studies [29,39–42] suggested an

66   involvement of the temporal cortex in face perception, they triggered a debate on

67   whether the occipito-temporal specialization for face perception in dogs matches that

68   of humans [29,39–42]. Previous work reported increased activation for faces

69   compared to objects [40,42], scenes [40], or a mono-coloured surface [39], but not

70   compared to other low-level visual controls (i.e., scrambled images [39,40] or the

71   back of the head [29]). Some studies lacked non-facial controls entirely [41]. Studies

72   additionally investigating responses to con- and heterospecifics were inconclusive

73   ranging from reports of increased responsiveness to dog stimuli in general (i.e., face

74   and back of the head) but no specialization for faces [29], over separate brain

75   regions specialized for human or dog faces [41], to no species- but general face-

76   preference [40]. Further, no previous work investigated the neural bases of body

77   perception. This is a major limitation, as bodies play an important role for social

78   perception in general, but in particular for dogs - as indicated e.g., by dogs' high

79   responsiveness to emotional or ostensive-referential bodily cues, such as tail-

80   wagging [43] or human gestures [43–45]. It is particularly noteworthy in this respect,

81   that dogs even outperform humans' closest living relatives, chimpanzees, in utilizing
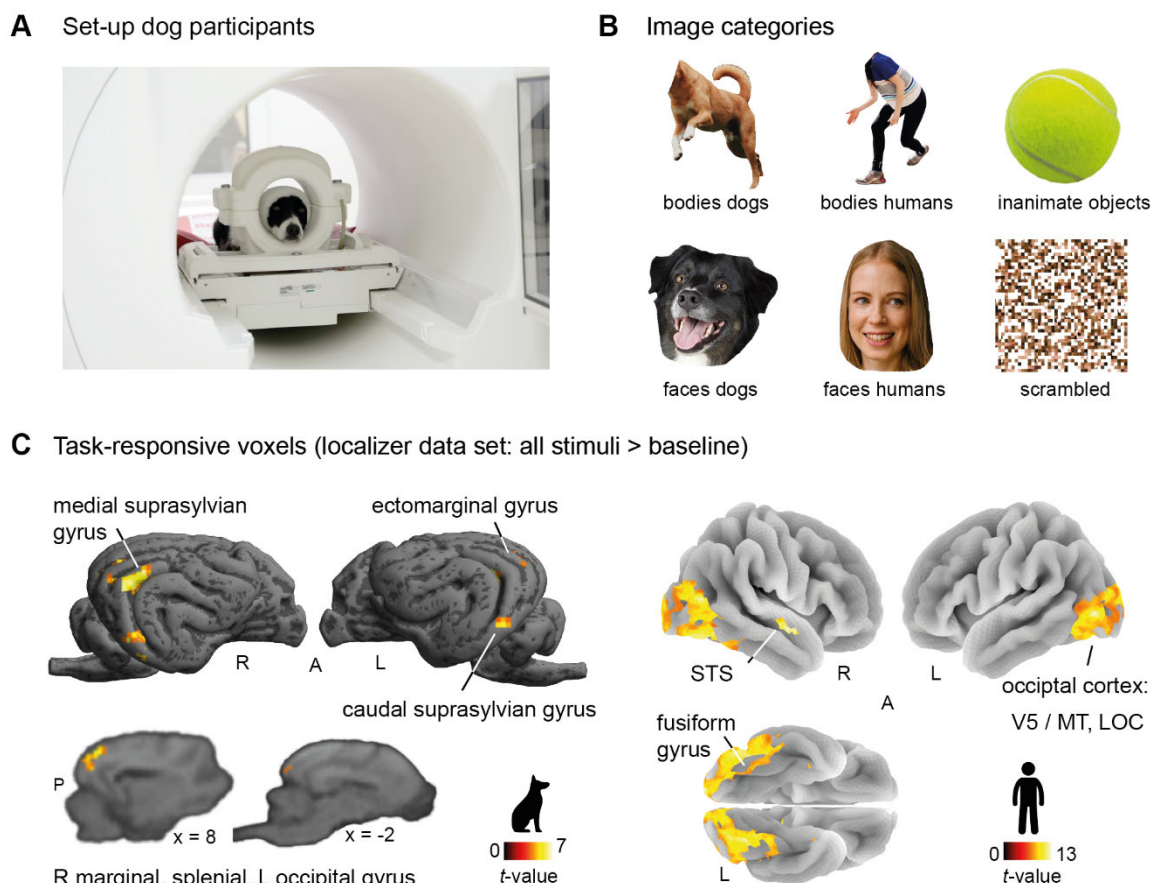
82   human ostensive cues [46].

83   Thus, the findings so far do not allow for a distinction between face and body or

84   general animacy perception and are inconclusive regarding the influence of the other

85   individual's species-identity. The present comparative neuroimaging study aimed to

4

86   resolve this debate. We performed the, to our knowledge, first systematic comparison

87   of the neural bases of face, body and inanimate object perception in dogs and

88   humans, in order to gain insights into how social perception has evolved in two

89   phylogenetically distant mammalian species [38,47].

2   Results

91   Fifteen awake and unrestrained pet dogs (**Fig 1A**) and forty human participants

92   underwent functional magnetic resonance imaging (MRI) while viewing images of

93   human and dog bodies, faces, inanimate objects (e.g., different toys), and grid-

94   scrambled versions of these images serving as visual controls (**Fig 1B**). Over the

95   course of two 5 min runs, participants saw 180 different images presented in a block

96   design interspersed with an implicit visual baseline. We analysed the dog fMRI data

97   with a newly developed analysis protocol shown to significantly improve neural signal

98   detection power [48]. All statistical tests were corrected for multiple comparisons (see

99   **fMRI data analysis**, **Fig 2**, **Tables S2-S3**).

Fig 1. *Overview of the comparative experimental approach to study the neural bases of face and body perception in dogs and humans.* (**A**) We obtained all imaging data using a 3T Siemens Skyra MR-system, equipped with a 15-channel human knee coil to scan the dog participants, and using a 32-channel human head coil for the human participants (not depicted). Dogs received extensive training [49] to stay motionless without restraints or sedation and could leave the MR scanner at any time via a custom-made ramp positioned at the scanner bed. All (dog and human) participants wore earplugs for noise protection and dog participants had an additional head bandage to secure optimal positioning of the earplugs throughout the scan session. (**B**) All participants viewed images of human and dog bodies, human and dog faces, inanimate objects (e.g., toys) or grid-scrambled versions of these images presented in a block design. (**C**) We split the data sets and used data from the first task run to compare activation for visual stimulation (all stimuli) to the visual baseline (i.e., the localizer data set). In both participant samples, we observed activation in the occipito-temporal cortices. These task-responsive voxels then served as a search space to determine individual functional regions-of-interest (fROIs), additionally constrained by bilateral anatomical regions (see **Fig 2A**). Results are displayed at $p < 0.05$, *FWE*-corrected at cluster-level using a cluster-defining threshold of $p < .001$ (dogs, Table S1), and $p < 0.05$ whole-brain *FWE*-corrected (humans; **Table S1**) Results for the dogs are overlaid onto a canine breed-averaged surface render [50], and onto the FreeSurfer "FsAverage" surface for humans (https://surfer.nmr.mgh.harvard.edu/fswiki). Anatomical nomenclature for all figures refers to the dog brain atlas from Czeibert and colleagues [51] and to the human brain atlas from the Laboratory for Neuro Imaging (LONI) Brain Atlas [52] (LPBA40; http://www.loni.usc.edu/atlases/). R, right; L, left; A, anterior; P, posterior; STS, superior temporal sulcus; MT, middle temporal visual area (V5); LOC, lateral occipital complex.

2.1 Mass-univariate analysis: Face- or body-sensitive areas in the occipito-temporal cortices of dogs and humans

To start out, we investigated whether dogs and humans have specialized cortical

regions for face and body perception, and whether these regions responded differently

to images of con- or heterospecifics. To this end, we used a standard functional region-

of-interest analysis approach (fROI,[53–55]). We split the data into two orthogonal data

sets, (1) a localizer data set (first task run) to define potential face- or body-sensitive

107   areas in visual-responsive brain regions (**Fig 1C, 2A**) and (2) a test data set (second

108   task run) to extract activation levels from these regions and to test potential category

109   sensitivity. We chose this approach for two reasons. First, we aimed at directly testing

110   the potential category-sensitivity, quantified by increased activation levels. Second, our

111   goal was to account for differences in the location of activation peaks between

112   individuals as reported in previous dog imaging studies [40,42].

2.1.1 Functional regions-of-interest (fROIs)

114   For each participant, we defined bilateral fROIs within constrained search spaces

115   to preserve spatial information (i.e., the rough anatomical location of activation peaks).

116   For the human participants, we used previously reported anatomical regions known to

117   be engaged in face and body perception [56]: the extrastriate body area, fusiform body

118   area, occipital face area and fusiform face area (**Fig 2A**). For the dog participants, we

119   could not build on previous research due to lack of shared template space and

120   availability of data. Therefore, we first compared activation levels associated with the

121   visual presentation of all stimuli compared to implicit baseline (i.e., white cross

122   presented on grey background) using the localizer data set. This revealed task-

123   responsive activation within the occipital-, splenial-, ectomarginal-, caudal-, medial

124   suprasylvian- and marginal gyri, partially overlapping with results from previous studies

125   investigating face perception [29,39–42,57,58] (**Fig 1C**, **Table S1**). We then used

126   anatomical masks [51] of these regions as search spaces for the dog participants (**Fig**

127   **2A**). For comparison, we also report task-responsive voxels for the human participants,

128   confirming involvement of the occipito-temporal cortex including the lateral occipital

129   cortex and fusiform gyrus (**Fig 1C**, **Table S1**; see also **Fig. S1** for schematic figures of

130   the dog and human brain).

131   We then defined individual category-sensitive regions within each search space

132   by selecting the top-10% voxels with the strongest activation for bodies or faces

133   compared to inanimate objects based on the individual data from each participant.

2.1.2 Sensitivity for animate stimuli but sub-division in face- and body-sensitive regions exclusive to humans

136   Next, we extracted the mean activation signal during viewing of faces, bodies,

137   inanimate objects and scrambled images (all compared to the implicit baseline) from

138   the individual fROIs using the test data set. In dogs, we observed significantly

139   increased activation levels for faces and bodies compared to inanimate objects or

140   scrambled images in both face and body fROIs, located in the medial and caudal

141   suprasylvian- and ectomarginal gyrus. In the caudal suprasylvian face- and

142   ectomarginal body fROI, the increased activation for faces showed the same trend but

143   did not always reach significance. We did not find consistent evidence for a further

144   sub-division into face- and body-selective areas in the occipito-temporal cortex, as

145   there was no significant activation difference between faces and bodies in seven out

146   of eight fROIs. We only observed significantly increased activation for bodies

147   compared to faces in the caudal suprasylvian face but not body fROI. The occipital and

148   splenial face and body fROIs did not result in differential activation changes in

149   response to any of the stimulus categories (**Table S2**). Regarding the parietal cortex,

150   the marginal gyrus appeared solely responsive to bodies compared to all other

151   conditions with no activation differences for faces compared to inanimate objects or

152   scrambled controls (**Fig 2B**).

153   Results for the human participants confirmed earlier research [10,11,24–

154   28,12,13,15–17,21–23] with the strongest overall activation levels for bodies in the

155   extrastriate and fusiform body areas and for faces in the occipital and fusiform face

156   areas (**Fig 2B**; **Table S2**). In summary, we found multiple occipito-temporal regions in

157   the dog and human cortices responsive to animate stimuli, but detected a further sub-

158   division into face- and body-sensitive regions exclusively in the human brain (see also

159   **Fig S1** for a summary of the results).

2.1.3 Conspecifics preference in human extrastriate body and fusiform face area
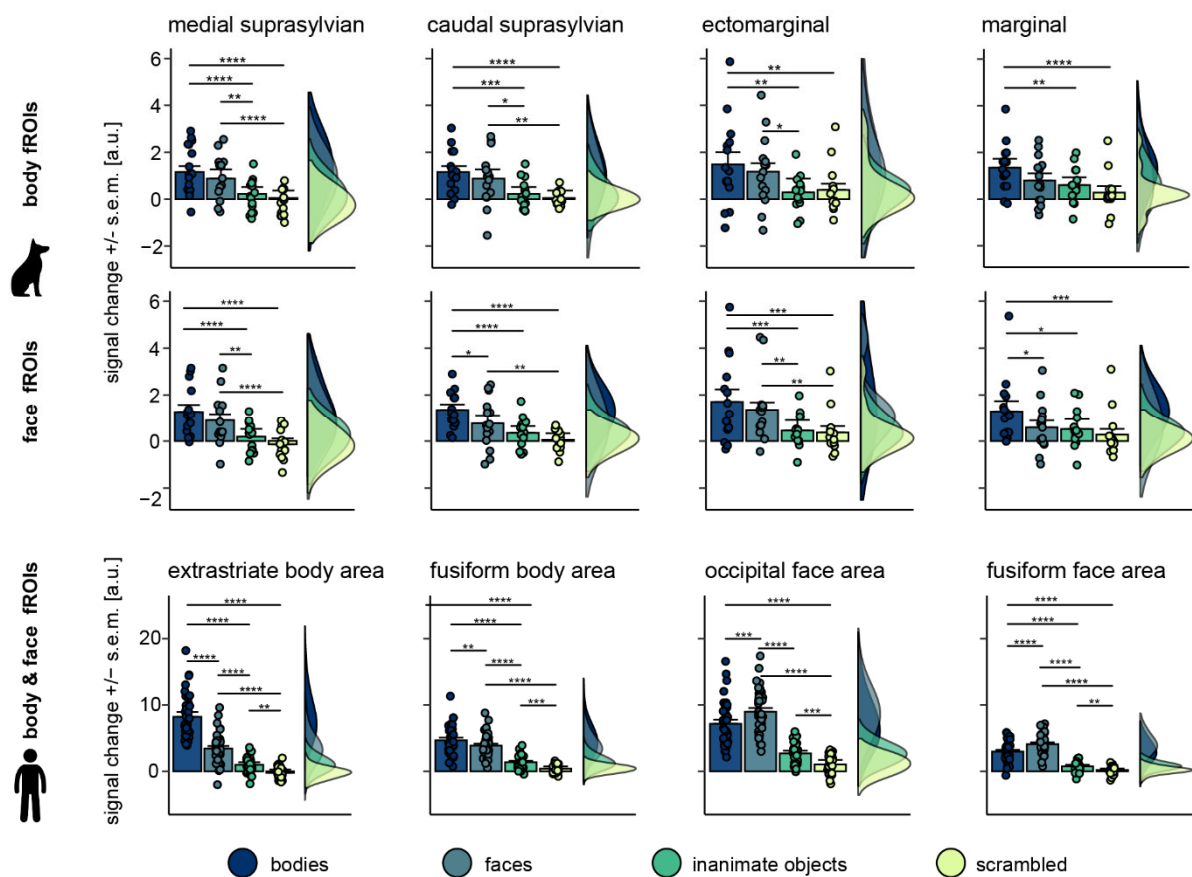
162   Next, we investigated whether processing of faces or bodies differed when

163   participants saw images of con- compared to heterospecifics (**Table S3**). In humans,

164   this revealed increased activation for human (mean: 4.46, *SD* = 1.83) compared to dog

165   bodies (mean: 3.76, *SD* = 1.66) in the extrastriate body area ($t(39) = 3.14$, $p = 0.003$),

166   as well as a general activation increase for human (mean: 1.89, *SD* = 0.87) compared

167   to dog (mean: 1.64, *SD* = 0.81) stimuli in the fusiform face area ($t(79) = 3.71$, $p <$

168   0.0001). For the dogs, we did not find a difference between the perception of dog and

169   human stimuli.
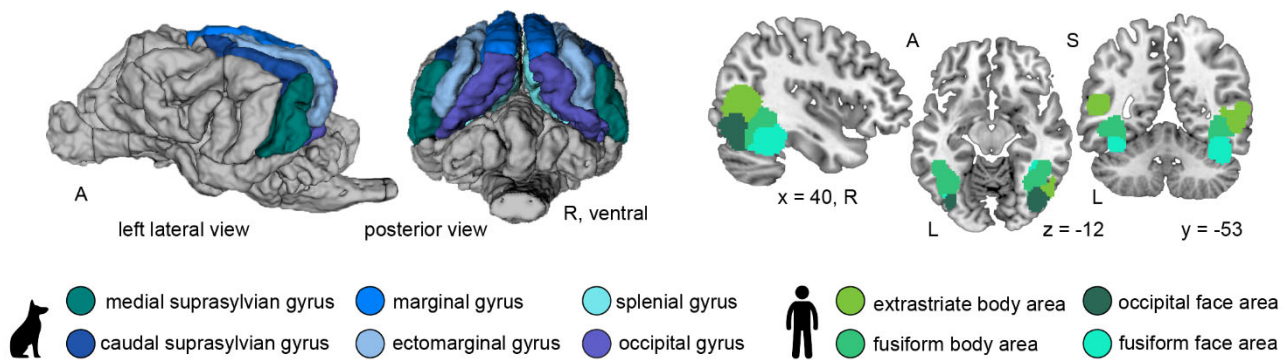
Fig 2. *Strongest activation levels for animate stimuli in both species, but differences between faces and bodies exclusive in humans.* (**A**) Based on the localizer data set, we defined individual category-specific regions-of-interest (functional region-of-interest approach, fROI) within multiple anatomically constrained search spaces using the contrasts bodies > inanimate objects (body fROIs) and faces > inanimate objects (face fROIs). (**B**) From these individual fROIs, we then extracted activation estimates during the viewing of faces, bodies, inanimate objects and scrambled images (all compared to the implicit baseline) using the data from the independent test data set to test potential face- or body-sensitivity. (**B**) In dogs, we observed increased activation levels for faces and bodies compared to inanimate objects or scrambled images in three occipito-temporal regions (medial and caudal suprasylvian, ectomarginal gyrus) in face and body fROIs. However, no difference between faces and bodies except in the caudal suprasylvian face fROI. The face and body fROIs located in the occipito-parietal marginal gyri resulted in increased activation levels primarily for bodies. In humans, similar to dogs, we observed the strongest activation levels for faces and bodies in all fROIs. In contrast to the dog data, the human data analysis consistently resulted in a significant activation change for bodies compared to faces in body fROIs and vice versa (**Table S2**). Planned comparisons were corrected for multiple comparisons using Tukey method. *p < .05, **p < .01, ***p < .001, ***p < .0001, s.e.m., standard error of the mean; a.u., arbitrary units. Atlas maps and search spaces refer to the dog brain atlas from Czeibert and colleagues [51] and human parcels were retrieved from previous work [56]. A, anterior; P, posterior; S, superior; L, left; R, right

170

171

2.2 Multivariate pattern analysis of animacy perception

Despite the overall activation (measured using mass-univariate analyses) to stimulus categories may not differ, we reasoned that more fine-grained analyses of multivariate activation patterns could reveal distinctions [59]. Therefore, we investigated the neural representations of faces and bodies in dogs and humans and their potential correspondence using whole-brain representational similarity analyses (RSA). We moved a 4 and 8 mm searchlight across the whole dog and human brain, respectively, in order to determine individual pattern similarity maps between all trials of each stimulus category [60–62] (**Fig 3A**). On the group-level, we then conducted paired *t*-tests to compare the pattern similarities maps of (1) animate vs. inanimate stimuli, (2) bodies vs. inanimate objects, (3) faces vs. inanimate objects, (4) faces vs. bodies, and (5,6) within the face and body categories: images of conspecifics vs. heterospecifics (i.e., dog faces vs. human faces; dog bodies vs. human bodies).

Results revealed increased (within-category) pattern similarity for animate compared to inanimate stimuli in the occipito-temporal cortex of dogs (i.e., caudal suprasylvian and splenial gyrus) and humans (i.e., middle occipital gyrus) overlapping with the identified fROIs. In human participants, we additionally observed increased similarity in the cerebellum and fronto-parietal regions (**Tables S4-S5**). In brief, this indicates distinct neural representations of animate compared to inanimate stimuli in higher-order visual regions of both species.

2.2.1 Similar and divergent neural representations for bodies and faces

Moving on to neural representations for bodies and faces, for bodies we observed increased pattern similarity compared to inanimate objects in higher-order visual areas in the occipito-temporal cortex, partially overlapping with the identified fROIs, and the cerebellum in both species (**Fig 3B**). Within the same regions (and again, in both
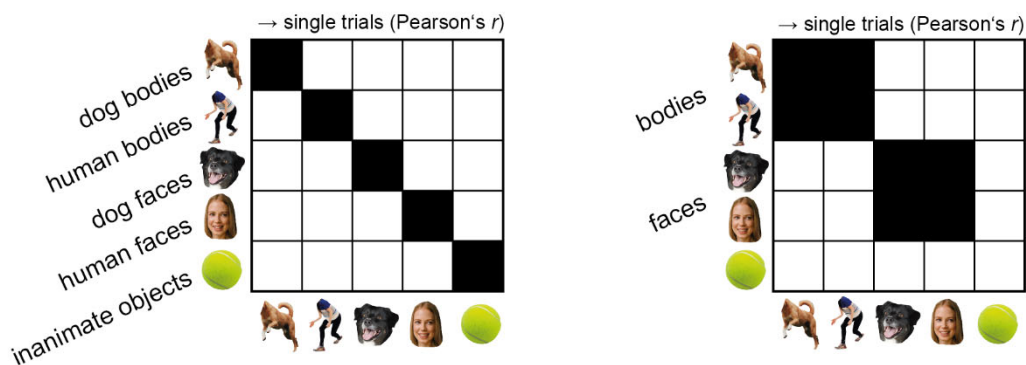
198   species), we also observed distinct activation patterns for conspecific compared to

199   heterospecific bodies. Furthermore, when the dogs viewed dog bodies, results

200   revealed increased similarity in limbic structures and regions associated with olfaction

201   (**Fig 3C**). In humans, we observed increased similarity for human compared to dog

202   bodies in fronto-parietal regions associated with action perception [63–65] (**Fig 3C**).

203   Observing faces compared to inanimate objects resulted in significantly

204   increased pattern similarity in occipito-temporal cortices of both species and again in

205   dog olfactory structures (**Fig 3D**). Comparing similarity patterns for faces vs. bodies,

206   we only found significant differences for the human participants (see **Tables S4-5** for

207   detailed results and **Fig S1** for a schematic summary of the main results).
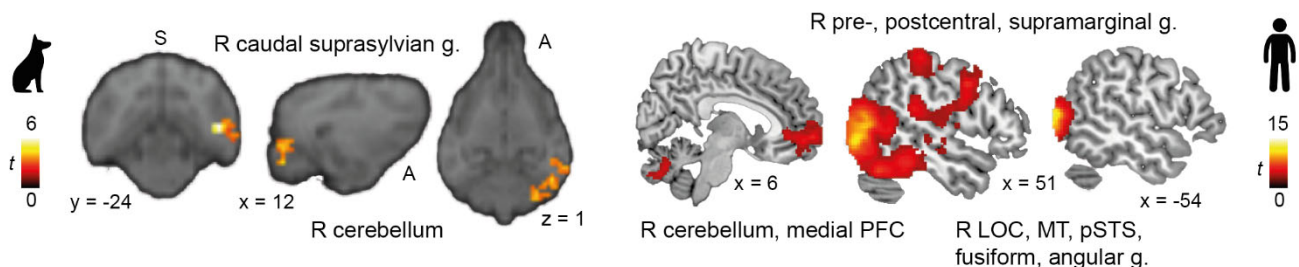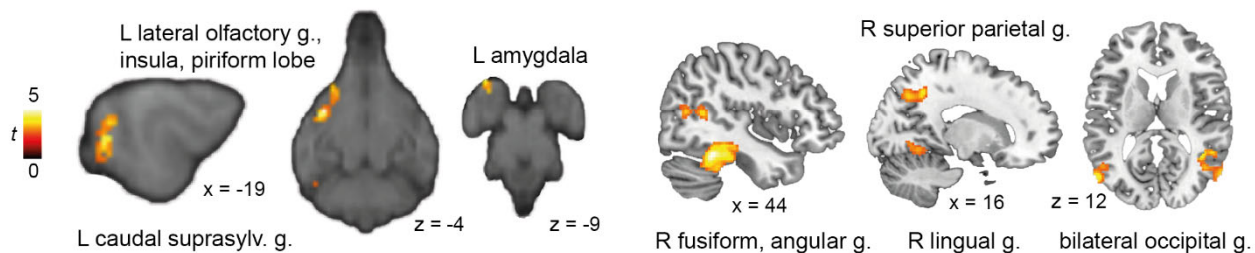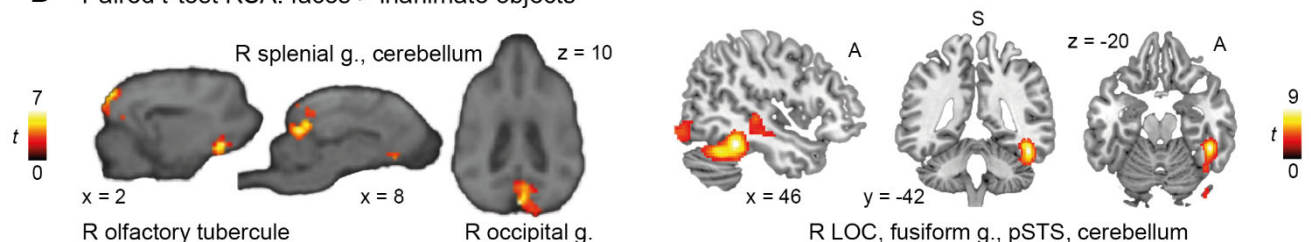
Fig 3. *Whole-brain representational similarity analysis (RSA) revealed similar and divergent neural patterns of activation for animate vs. inanimate stimuli but differences between faces and bodies again exclusive in human.* (**A**) We moved a 4/8 mm (dog/human) spherical searchlight across the whole brain to quantify the neural patterns underlying stimuli categories. Pattern similarity matrices were computed across the respective quadrants marked in black. (**B,D**) In both species, we observed increased pattern similarity for bodies or faces compared to inanimate stimuli in higher-order visual areas in the occipito-temporal cortex and the cerebellum. (**C,D**) In dogs we additionally detected distinct neural patterns of activation for faces and conspecific (= dog) bodies in olfactory and limbic regions. In humans, we observed an increased pattern similarity for (conspecific) bodies in fronto-parietal regions associated with action perception [63–65]. All results are displayed at $p < 0.05$ *FWE*-corrected at cluster-level, and using a cluster-defining threshold of $p < .005$ for the dog and $p < .001$ for the human data (**Tables S4-5**). Anatomical locations are shown in panel B for the dog and in D for the human data: superior (S), anterior (A); all sagittal, coronal and axial planes displayed have the same orientation. Coordinates refer to a canine-breed averaged template [50] or to MNI space for the human data. Person's *r*, correlation coefficient; t, *t*-value; g., gyrus; PFC, prefrontal cortex LOC, lateral occipital cortex; MT, middle temporal visual area (V5); pSTS, posterior superior temporal sulcus; R, right; L, left.

208

3   Discussion

Our findings revealed that the occipito-temporal cortex has a prominent role in the perception of animate entities in both dogs and humans. This suggests that the neural processing of animate vs. inanimate stimuli across mammalian brains may either have an old evolutionary origin in the common ancestors of canines and primates or is the result of convergent evolution [47]. However, within these regions, only humans displayed an additional sub-division into distinct face- and body-sensitive brain regions. Moreover, only dogs showed distinct responses to human and dog faces as well as dog bodies in olfactory areas (see **Fig S1** for summary of the results). These findings suggest a divergent evolution of the neural bases of face and body perception (or processing) in dogs and humans. The differential engagement of visual and olfactory brain functions would fit particularly well with the differential sensitivity and preferential use of these perceptual systems to infer social and contextual information.

Detecting biological agents is crucial for survival and social relationships. Hence, the visual differentiation between animate vs. inanimate entities is an evolutionary important category representation. Studies show that dogs target animate agents when, for example, presented with images of wild animals, humans or dogs embedded in natural landscapes [66] or of social interactions between humans and dogs [67]. Further, dividing stimuli into an animate vs. inanimate dimension is one of the first visually salient categorizations formed by human infants [68]. In this way, animacy representation provides the first building block for more complex visual categorizations such as faces vs. bodies. Thus, considering its biological significance and the observed cross-species similarities in our study, animacy might constitute a general organizing principle across mammalian brains.

Behavioural [7,33,34,43,69–72] and imaging studies [57,58] have also demonstrated that dogs are able to perceive facial and bodily cues of dogs and humans

235   and display high responsiveness to ostensive-referential bodily cues [44,45,73,74],

236   already as puppies [75]. Our results do not contradict these findings, but suggest that

237   visual regions involved in the perception of faces are also involved in the perception of

238   other body parts, and may thus encode animate stimuli. A recent dog neuroimaging

239   study [76] also showed that the visual regions observed in our study play a crucial part

240   in the perception of complex social interactions, which would confirm their important

241   role for social perception.

242   While previous investigations of how dogs perceive bodies have mainly focused

243   on the decoding of human referential cues, we hope that our work will inspire more

244   research on how dogs perceive bodily social as well as emotional cues of con- as well

245   as heterospecifics. The absence of a further sub-specialization for face vs. body

246   perception in the occipito-temporal cortex of dogs might indeed indicate that dogs in

247   comparison to humans focus more on whole body social cues rather than on specific

248   sub-parts. This interpretation is notably well in line with a recent comparative eye-

249   tracking study [77].

250   Regarding species perception, our results indicate an increased salience for

251   human compared to dog stimuli in humans, but no evidence for a conspecific-

252   preference in the occipito-temporal cortex of dogs. Thus, human and dog stimuli

253   appear to be equally salient for dogs. This is in line with previous behavioural studies

254   suggesting, for example, no significant difference in the perception of human or dog

255   emotional facial [34], whole-body cues [77], or images of social interactions [67].

256   Further, two recent studies demonstrated that dogs, already as puppies, follow human

257   gestural-communication and show an interest in human faces [75], which has not been

258   observed in wolf puppies [78]. Additionally, half of the variation in these socio-cognitive

259   skills could be accounted for by genetic factors, suggesting that dogs' attention to

260   humans might have been enhanced during domestication [75 for review of both

261 studies]. Future studies investigating species-preferences in dogs might thus consider

262 adding further heterospecific stimuli of other familiar species, such as cats.

263 In accordance with a potential divergent evolution of face and body

264 representations in dogs and humans, we also observed distinct neural representations

265 for faces (regardless of species) and conspecific (dog) bodies in dog olfactory regions.

266 Although unexpected, these results might reflect dogs' significantly higher olfactory

267 sensitivity and its use to infer social and contextual information [54 for review].

268 However, the link between cognition and olfaction remains speculative since

269 behavioural studies using olfactory cues so far mainly explored dogs' odour and

270 disease detection abilities (e.g., [81–85]), while dog imaging studies on olfaction

271 focused on reward-processing [86,87] or general sensory abilities [88–90]. However,

272 a recent behavioural study investigating dog cognition using olfactory cues showed

273 first evidence that dogs form representations of their owners when smelling their tracks

274 [91].

275 In humans, results revealed distinct activation patterns for bodies in fronto-

276 parietal regions that have been consistently associated with the perception of actions

277 [63–65]. In dogs, we did not find activation in (pre-)motor cortices, but the increased

278 neural sensitivity for bodies in the occipito-parietal marginal gyrus might be initial

279 evidence for an analogous visual pathway to encode actions. However, this is beyond

280 our study's scope, and the precise neural underpinnings of action observation in dogs

281 have not yet been investigated.

282 We have taken several steps to maximize neural signal sensitivity already when

283 designing our study (e.g., by using a block design) and at the analysis stage (e.g., by

284 using dog-tailored hemodynamic models increasing response detection power [48]).

285 Nevertheless, the extensive training required for dogs [49] resulted in different sample

286 sizes for the two species, and the more extensive prior work in humans [56] resulted

287   in more constrained search spaces, and likely higher spatial sensitivity for the human

288   data. Further, the majority (80%) of our pet dogs were pure-bred herding dogs, which

289   prevented us from testing potential breed-specific differences and may limit

290   generalizability.

291   In conclusion, our study reveals novel evidence for similarities and differences of

292   animacy perception between two phylogenetically distant mammal species, advancing

293   our understanding of the foundations of social cognition and behaviour. Finally, we

294   provide insights into the differentially evolved sensory systems of dogs and humans

295   for the perception of faces and bodies.

4   Materials and Methods

4.1 Participants

298   Fifteen pet dogs (*Canis familiaris*; 11 females, age range: 4-11 years, mean age:

299   7.8 years) consisting of 10 Border collies, 2 Australian shepherds, 1 Labrador retriever

300   and 2 mixed-breed dogs and forty human participants (22 females, age range: 19-28

301   years, mean age: 23 years) participated in the present study.

302   Prior to MRI scanning, all dogs underwent initial medical examination concerning

303   their eyesight and general health and received extensive training to habituate to the

304   MRI environment [49]. They were fully awake, able to exit the MRI scanner at any time

305   and equipped with noise protection (**Fig 1A**). All caregivers gave informed written

306   consent to their dogs' participation. Human participants were right handed, had normal

307   or corrected-to-normal vision, they reported no history of neurological or psychiatric

308   disease, nor phobia of dogs, fulfilled the standard inclusion criteria for functional MRI,

309   and gave informed written consent to participate. Dog data collection was approved by

310   the institutional ethics and animal welfare commission in accordance with Good

311   Scientific Practice (GSP) guidelines and national legislation at the University of

312   Veterinary Medicine Vienna (ETK-06/06/2017), based on a pilot study conducted at

313   the University of Vienna. Human data collection was approved by the ethics committee

314   of the University of Vienna (reference number: 00565) and performed in line with the

315   latest revision of the Declaration of Helsinki (2013).

316   ## 4.2 Task and procedure

317   We employed a block design (duration: 12 s) split in two 5 min runs where

318   participants saw images of faces and bodies of dogs or humans, objects and

319   scrambled versions of these images (5 images per block; **Fig 1B**, see below) on an

320   MR-compatible screen (32 inch) positioned at the end of the scanner bore. Crucially,

321   we used the same task for dogs and humans. Human participants were instructed to

322   watch the images presented on the MR screen and dogs were trained to attend to the

323   MR screen (passive viewing paradigm). Each run contained three blocks per condition,

324   block order was randomized but the same condition was never presented twice in a

325   row. Between blocks, participants saw a visual baseline jittered between 3-7 s with a

326   white cross presented on a grey background. Image composition for each block and

327   order within each block was randomized across participants to ensure effects are not

328   driven by specific blocks; each image was presented once. The task was implemented

329   using PsychoPy [92]. Overall motion and wakefulness were live monitored via the

330   camera of an eye-tracker (Eyelink 1000 Plus, SR Research, Ontario, Canada)

331   positioned below the MR-compatible screen. For the dogs, the trainer stayed within the

332   scanner room but out-of-sight throughout the scan session to monitor and handle the

333   dogs. Human participants saw both runs within a single scanner session with a short

334   break in-between. For the dogs, the number of attempted sessions varied depending

335   on how many repetitions they needed to complete one run without substantive motion

336   and with sufficient attentiveness (i.e., eyes open and gazing towards the centre of the

337   screen); in-between task runs the dogs always were given a short break outside the

338   MR scanner. Realignment parameters were evaluated after each scan session. If

339   overall motion exceeded 4 mm in any of the three translation directions, the dog was

340   re-invited to repeat the run in a subsequent session and sessions were scheduled at

341   least one week apart. On average, dogs needed three sessions to complete both runs.

342   No data of the non-successful sessions were used for analysis.

4.2.1 Stimulus material

344   The stimulus set comprised 180 coloured images of faces and bodies of dogs

345   and humans, everyday inanimate objects (e.g., a toy, a chair), and phase-grid

346   scrambled versions of each category (30 images per condition) derived from Wagner

347   and colleagues [93], the Hemera Photo-Object data base (Hemera Technologies) and

348   the internet (see **Fig 1B** for examples). The images were resized to 600 × 600 pixels

349   and presented in the centre of the MR screen on grey background. We cut out the

350   heads off from the body images, as well as objects from body images (e.g., a coffee

351   cup, a soccer ball). The images showed a variety of postures (e.g., jumping, looking

352   up), neutral and positive emotional displays (e.g., sleeping, smiling) and viewing

353   perspectives (e.g., from above, from a side angle). Luminance was set homogeneously

354   across stimuli and we controlled for spatial extent (see supporting information for

355   details).

4.3 MRI data acquisition

357   We acquired all MRI data with a 3T Siemens Skyra MR-system (Siemens

358   Medical, Erlangen, Germany) and a 15-channel coil (initially designed for

359   measurements of the human knee) for data acquisition in dogs and a 32-channel

360   human head coil for data acquisition in humans. Functional scans of dogs used a 2-

361   fold multiband (MB) accelerated echo planar imaging (EPI) sequence including the

362   following parameters: voxel size = 1.5 x 1.5 x 2 mm^3, repetition time (TR) / echo time

363   (TE) = 1000/38 ms, field of view (FoV) = 144 × 144 × 58 mm^3, flip angle = 61°, 20%

364 gap and 24 axial slices covering the whole brain (interleaved acquisition, descending

365 order). Structural scans had a voxel size of 0.7 mm isotropic (TR/TE = 2100/3.13 ms,

366 FoV = 230 × 230 × 165 mm^3) and were acquired in a separate scan session prior to

367 functional data collection. Human functional scans were acquired using a 4-fold MB

368 accelerated EPI sequence including the following parameters: voxel size = 2 mm

369 isotropic, TR/TE = 1200/34 ms, FoV = 192 × 192 × 124.8 mm^3, flip angle = 66°, 20%

370 gap and 52 axial slices coplanar to the connecting line between anterior and posterior

371 commissure (interleaved acquisition, ascending order). Additionally, we obtained field

372 map scans to correct functional scans for magnetic field inhomogeneities using a

373 double echo gradient echo sequence with the following parameters: voxel size = 1.72

374 x 1.72 x 3.85 mm^3, TR/TE1/TE2 = 400/4.92/7.38 ms, FoV = 220 × 220 × 138 mm^3, flip

375 angle = 60° and 36 axial slices (same orientation as functional scans). Structural scans

376 had a voxel size of 0.8 mm isotropic (TR/TE = 2300/2.43 ms,

377 FoV = 256 × 256 × 166 mm^3) and were acquired after functional data acquisition.

378 **4.4 Data processing and statistical analysis**

379 Imaging data was preprocessed and analyzed using SPM12

380 (https://www.fil.ion.ucl.ac.uk/spm/software/spm12/), Matlab 2018b (MathWorks) and R

381 3.6.3 [94].

382 **4.4.1 MRI data preprocessing**

383 In both samples, we slice-time corrected (reference: middle slice) and realigned

384 functional images to the mean image. Human imaging data was also unwarped using

385 the acquired field map. Dog imaging data was manually reoriented with the rostral

386 commissure set as a visual reference (SPM module: "*Reorient images / Set origin*") to

387 match the template orientation [50] and structural images were skull-stripped using

388 individual binary brain masks created using itk-SNAP [95]. Next, we co-registered the

389   structural and functional images to the mean functional image, segmented the

390   structural images in both samples and normalized the human data to the Montreal

391   Neurological Institute (MNI) template space and the dog data to a breed-averaged

392   stereotaxic template space [50]. Normalized images were resliced to 1.5 mm isotropic

393   and smoothed with a 3-dimensional Gaussian kernel (full-width-at-half-maximum,

394   FWHM; with twice the raw voxel resolution: dogs/humans = 3/4 mm; see [48] for an in-

395   depth description of our dog data preprocessing pipeline). We then calculated

396   individual scan-to-scan motion (frame wise displacement, FD) and added motion

397   regressors to first-level GLMs for each scan exceeding the a priori set FD threshold of

398   0.5 mm (motion scrubbing [96,97]) to account for both translational and rotational

399   displacements. For the dog participants, we removed on average 8% of the scans from

400   each run (run 1: mean FD = 0.23 mm, 90th percentile = 0.36 mm; run 2: mean FD =

401   0.24 mm, 90th percentile = 0.38 mm) and 1% of the scans from each run of the human

402   participants (run 1: mean FD = 0.17 mm, 90th percentile = 0.22 mm; run 2: mean FD =

403   0.18 mm, 90th percentile = 0.21 mm).

404   4.4.2 fMRI data analysis

405   **Mass-univariate activation analysis**. We analysed the functional data using a

406   general linear model (GLM) approach implemented in SPM12. Individual GLM

407   matrices included six regressors of interest for task (dog faces, dog bodies, human

408   faces, human bodies, inanimate objects, scrambled) and the six regressors from the

409   realignment procedure (see above) were added as nuisance regressors. All blocks

410   were estimated using a boxcar function time-locked to the onset of each block with a

411   duration of 12 s. For the dog data, the signal was convolved with a tailored dog

412   haemodynamic response function [48] (HRF), while the standard human canonical

413   HRF (i.e., the default HRF parameters provided by SPM12) was used for the human

414   data. The dog HRF reflects a previously observed 2-3 s earlier peak of the BOLD signal

415 than expected by the human HRF model [48]. Normalized, individual binary masks

416 served as explicit masks and we applied a high-pass filter with a cut-off at 128 s. We

417 then split the data in two sets (task run 1, task run 2). Based on the data from the first

418 task run, we estimated three subject-level contrast maps for the difference between

419 our conditions of interest (i.e., faces, bodies with equal weights for human and dog

420 images) and objects, and a visual stimulation contrast (all conditions > implicit visual

421 baseline). For the second task run, we computed eight subject-level contrasts, one for

422 each task regressor (i.e., dog bodies, human bodies, dog faces, human faces,

423 everyday inanimate objects, scrambled), averaged for faces (i.e., dog and human

424 faces) and averaged for bodies (i.e., dog and human bodies) compared to implicit

425 visual baseline.

426 **Functional region of interest (fROI) approach.** We implemented a standard

427 functional region-of-interest (fROI, [53–55]) approach to investigate potential category-

428 specificity of cortical regions. This approach allows us to directly test the potential

429 category-sensitivity quantified by increased activation level while accounting for slight

430 differences in the location of activation peaks between individuals as which have been

431 reported in previous dog imaging studies [40,42].

432 The participant-level contrast images from the first run served as localizer data to

433 define individual category-sensitive regions. Within anatomically constrained search

434 spaces (**Fig 2A**) we selected the top-10% voxel from each hemisphere with the

435 strongest signal for the condition-of-interest (i.e., face areas: faces > objects, body

436 areas: bodies > objects) to form bilateral individual fROIs. Selecting the top-10% voxel

437 was an *a priori* decision we made because the resulting fROI sizes (on average: 30

438 voxels) were similar to the average cluster size observed in a previous dog imaging

439 study that used two visual paradigms and the same smoothing kernel [48]. Further,

440 percentages instead of absolute numbers took also the varying search space sizes

441   into account (see **supporting material** and **Fig S2-3** for more information). The data

442   from the left out second task run allowed then to directly test potential category

443   specificity in an independent data set. Thus, we extracted the activation levels from the

444   conditions-of-interest contrasted against implicit visual baseline from both body and

445   faces areas (= individual fROIs).

446   Group functional ROI analyses were performed running repeated measures

447   analyses of variance (ANOVAs). First, we tested our main research question, whether

448   the body areas resulted in increased sensitivity for bodies regardless of species and

449   vice versa for faces, and added everyday objects and scrambled images as further

450   conditions. Thus, we ran a one-way ANOVA with *stimuli category* (faces, bodies,

451   everyday objects, scrambled*)* as dependent variable. Next, to investigate if there is a

452   difference in activation between conspecific and heterospecific stimuli, we used 2 x 2

453   within-subjects ANOVAs (*species*: conspecific, heterospecific; *image category*: face,

454   body). *P*-values for group comparisons investigating the same research questions

455   were Bonferroni-adjusted, e.g., if the 6 potential body fROIs result in increased

456   sensitivity for bodies compared to all other categories results in an adjusted *p*-value of

457   0.008 (= 0.05/6). Adjusted *p*-values are reported along with the results (**Tables S2-3**).

458   For whole-brain group analyses, we tested significance applying a whole-brain

459   familywise error (*FWE*) correction for the human data and a cluster-level inference with

460   a cluster defining threshold of $p < 0.001$ and a cluster probability of $p < 0.05$ *FWE*

461   corrected for multiple comparisons for the dog data. Cluster extent (i.e., minimum

462   spatial extend to be labelled significant) was calculated using the SPM extension

463   "CorrClusTh.m" (by Thomas Nichols, University of Warwick, United Kingdom, and

464   Marko   Wilke,   University   of   Tübingen,   Germany;

465   https://warwick.ac.uk/fac/sci/statistics/staff/academic-research/nichols/scripts/spm/).

23

466   **Representational similarity analysis**. Next, we investigated the neural

467   representations for faces, bodies and objects and their potential convergence in dogs

468   and humans. To this end, we performed a whole-brain representational similarity

469   analysis (RSA; [60–62]) to determine neural pattern similarities within image

470   categories. GLMs were modelled identical to univariate GLMs (see above) but for each

471   block, we ran a separate GLM with the block as task regressor and remaining blocks

472   were combined in one regressor of no interest [98]; runs were modelled independently.

473   Thus, the analysis resulted in 36 beta images for each participant (6 conditions × 6

474   trials). RSA was performed using the smoothed functional data. For all RSA analyses,

475   we moved a spherical searchlight [99] (dogs: r = 4 mm, 81 voxel; humans: r = 8 mm,

476   251 voxel) throughout individual whole-brain grey matter masks computed based on

477   the normalised segmentation output considering only searchlights with a minimum of

478   15 grey matter voxel for the dog and 30 for the human data.

479   Within a given searchlight, we extracted single-trial beta estimates from all voxels

480   and sorted them according to their stimuli category (**Fig 3A**; dog / human bodies, dog

481   / human faces, inanimate objects) and reshaped the data to a trial × voxel matrix. Next,

482   we *z*-scored the data across trials and runs and computed a trial × trial similarity matrix

483   by correlating each beta estimate of each trial to all other trial estimates. Finally, in

484   order to retrieve overall similarity scores, we then Fisher's *z*-transformed the data and

485   calculated overall similarity matrices by averaging scores across the respective

486   quadrants. We were specifically interested in pattern similarities across animate vs.

487   inanimate (faces × bodies vs. inanimate objects), faces or bodies vs. inanimate objects,

488   faces vs. bodies and conspecific vs. heterospecific species dimensions within face and

489   body categories. We then assigned the overall similarity values to the centre voxel of

490   each searchlight resulting in individual whole-brain pattern similarity maps.

491   On the group-level, we then used paired *t*-tests to compare the pattern similarities

492   between trials of (1) faces vs. inanimate objects (i.e., [dog faces × human faces] vs.

493   inanimate objects), (2) bodies vs. inanimate objects (i.e., [dog bodies × human bodies]

494   vs. inanimate objects), (3) animate vs. inanimate images (i.e., [dog faces × human

495   faces x dog bodies × human bodies] vs. inanimate objects), (4) faces vs. bodies (i.e.,

496   [dog faces × human faces] vs. [dog bodies × human bodies]), and (5,6) within the face

497   and body categories: images of conspecifics vs. heterospecifics (i.e., dog faces vs.

498   human faces; dog bodies vs. human bodies). We computed permutation tests [100] to

499   determine group-level significance using the Statistical nonParametric Mapping

500   (SnPm13) toolbox running 5000 permutations for each paired *t*-test and applied

501   cluster-level inference with a cluster defining threshold of *p* < .005/.001 (dogs/humans)

502   and a cluster probability of *p* < 0.05 familywise error corrected (*FWE*) for multiple

503   comparisons.

504   **Data   visualization**.   Data   was   visualized   using   SPM12

505   (https://www.fil.ion.ucl.ac.uk/spm/software/spm12/), Matlab 2018b (MathWorks), itk-

506   SNAP [95], R 3.6.3 [94] with mainly the packages ggplot2 [101] and RainCloudPlots

507   [102] and the python project nilearn (http://nilearn.github.io).

5   Acknowledgments

517   no role in study design, data collection and analysis, decision to publish, or preparation

518   of the manuscript.

6   CRediT authorship statement

520   **Magdalena Boch**: Conceptualization, Methodology, Software, Validation, Formal analysis, Investigation, Data curation, Writing - original draft, Writing - review & editing, Visualization, Project administration. **Isabella C. Wagner**: Conceptualization, Methodology, Resources, Writing - original draft, Writing - review & editing, Supervision. **Sabrina Karl**: Investigation, Writing - review & editing. **Ludwig Huber**: Conceptualization, Resources, Writing - review & editing, Supervision, Funding acquisition. **Claus Lamm**: Conceptualization, Methodology, Resources, Writing - original draft, Writing - review & editing, Supervision, Funding acquisition.

7   Declaration of Competing Interests

529   The authors declare no competing financial interests.

8 References

530

531

532   1.   Rajhans P, Jessen S, Missana M, Grossmann T. Putting the face in context: Body expressions impact facial emotion processing in human infants. Dev Cogn Neurosci. 2016;19: 115–121. doi:10.1016/J.DCN.2016.01.004

535   2.   Aviezer H, Trope Y, Todorov A. Body cues, not facial expressions, discriminate between intense positive and negative emotions. Science. 2012;338: 1225–1229. doi:10.1126/science.1224313

538   3.   Barrett LF, Mesquita B, Gendron M. Context in emotion perception. Curr Dir Psychol Sci. 2011;20: 286–290. doi:10.1177/0963721411422522

540   4.   Lecker M, Dotsch R, Bijlstra G, Aviezer H. Bidirectional contextual influence between faces and bodies in emotion perception. Emotion. 2020;20: 1154–1164. doi:10.1037/EMO0000619

542   5.   Poyo Solanas M, Zhan M, Vaessen M, Hortensius R, Engelen T, de Gelder B. Looking at the face and seeing the whole body. Neural basis of combined face and body expressions. Soc Cogn Affect Neurosci. 2018;13: 135–144. doi:10.1093/scan/nsx130

545   6.   de Gelder B, de Borst AW, Watson R. The perception of emotion in body expressions. Wiley Interdiscip Rev Cogn Sci. 2015;6: 149–158. doi:10.1002/wcs.1335

547   7.   Müller CA, Schmitt K, Barber ALA, Huber L. Dogs can discriminate emotional expressions of human faces. Curr Biol. 2015;25: 601–605. doi:10.1016/j.cub.2014.12.055

549   8.   Kravitz DJ, Saleem KS, Baker CI, Ungerleider LG, Mishkin M. The ventral visual pathway: An expanded neural framework for the processing of object quality. Trends Cogn Sci. 2013;17: 26–49. doi:10.1016/j.tics.2012.10.011

552   9.   Ungerleider LG, Haxby J V. "What" and "where" in the human brain. Curr Opin Neurobiol. 1994;4: 157–165. doi:10.1016/0959-4388(94)90066-3

554   10.   Schwarzlose RF, Baker CI, Kanwisher N. Separate face and body selectivity on the fusiform gyrus. J Neurosci. 2005;25: 11055–11059. doi:10.1523/JNEUROSCI.2621-05.2005

556   11.   Peelen M V., Downing PE. Selectivity for the human body in the fusiform gyrus. J Neurophysiol. 2005;93: 603–608. doi:10.1152/jn.00513.2004

558   12.   Peelen M V., Downing PE. The neural basis of visual body perception. Nat Rev Neurosci. 2007;8: 636–648. doi:10.1038/nrn2195

560   13.   Downing PE, Jiang Y, Shuman M, Kanwisher N. A cortical area selective for visual processing of the human body. Science. 2001;293: 2470–2473. doi:10.1126/science.1063414

562   14.   Spiridon M, Fischl B, Kanwisher N. Location and spatial profile of category-specific regions in human extrastriate cortex. Hum Brain Mapp. 2006;27: 77–89. doi:10.1002/hbm.20169

564   15.   Kanwisher N. Domain specificity in face perception. Nat Neurosci. 2000;3: 759–763. doi:10.1038/77664

566   16.   Yovel G, Kanwisher N. Face perception: domain specific, not process specific. Neuron. 2004;44: 889–898. doi:10.1016/j.neuron.2004.11.018

568   17.   Wegrzyn M, Riehle M, Labudda K, Woermann F, Baumgartner F, Pollmann S, et al. Investigating the brain basis of facial expression perception using multi-voxel pattern analysis. Cortex. 2015;69: 131–140. doi:10.1016/J.CORTEX.2015.05.003

571   18.   Wiggett AJ, Pritchard IC, Downing PE. Animate and inanimate objects in human visual cortex:
572   Evidence for task-independent category effects. Neuropsychologia. 2009;47: 3111–3117.
573   doi:10.1016/J.NEUROPSYCHOLOGIA.2009.07.008

574   19.   Chao LL, Haxby J V., Martin A. Attribute-based neural substrates in temporal cortex for
575   perceiving and knowing about objects. Nat Neurosci. 1999;2: 913–919. doi:10.1038/13217

576   20.   Downing PE, Chan AW-Y, Peelen M V., Dodds CM, Kanwisher N. Domain specificity in visual
577   cortex. Cereb Cortex. 2006;16: 1453–1461. doi:10.1093/CERCOR/BHJ086

578   21.   Kanwisher N, Yovel G. The fusiform face area: a cortical region specialized for the perception
579   of faces. Philos Trans R Soc B Biol Sci. 2006;361: 2109–2128. doi:10.1098/rstb.2006.1934

580   22.   Tsao DY, Freiwald WA, Tootell RBH, Livingstone MS. A cortical region consisting entirely of
581   face-selective cells. Science. 2006;311: 670–674. doi:10.1126/science.1119983

582   23.   Tsao DY, Moeller S, Freiwald WA. Comparing face patch systems in macaques and humans.
583   Proc Natl Acad Sci U S A. 2008;105: 19514–19519. doi:10.1073/pnas.0809662105

584   24.   Tsao DY, Freiwald WA, Knutsen TA, Mandeville JB, Tootell RBH. Faces and objects in
585   macaque cerebral cortex. Nat Neurosci. 2003;6: 989–995. doi:10.1038/nn1111

586   25.   Desimone R, Albright TD, Gross CG, Bruce C. Stimulus-selective properties of inferior
587   temporal neurons in the macaque. J Neurosci. 1984;4: 2051–2062. doi:10.1523/jneurosci.04-
588   08-02051.1984

589   26.   Wachsmuth E, Oram MW, Perrett DI. Recognition of objects and their component parts:
590   Responses of single units in the temporal cortex of the macaque. Cereb Cortex. 1994;4: 509–
591   522. doi:10.1093/cercor/4.5.509

592   27.   Gross CG, Bender DB, Rocha-Miranda CE. Visual receptive fields of neurons in inferotemporal
593   cortex of the monkey. Science. 1969;166: 1303–1306. doi:10.1126/science.166.3910.1303

594   28.   Haxby J V., Horwitz B, Ungerleider LG, Maisog JM, Pietrini P, Grady CL. The functional
595   organization of human extrastriate cortex: a PET-rCBF study of selective attention to faces and
596   locations. J Neurosci. 1994;14: 6336–6353. doi:10.1523/JNEUROSCI.14-11-06336.1994

597   29.   Bunford N, Hernández-Pérez R, Farkas EB, Cuaya L V., Szabó D, Szabó ÁG, et al.
598   Comparative Brain Imaging Reveals Analogous and Divergent Patterns of Species and Face
599   Sensitivity in Humans and Dogs. J Neurosci. 2020;40: 8396–8408.
600   doi:10.1523/JNEUROSCI.2800-19.2020

601   30.   Kanwisher N, Stanley D, Harris A. The fusiform face area is selective for faces not animals.
602   Neuroreport. 1999;10: 183–187. doi:10.1097/00001756-199901180-00035

603   31.   Pinsk MA, Arcaro M, Weiner KS, Kalkus JF, Inati SJ, Gross CG, et al. Neural representations
604   of faces and body parts in macaque and human cortex: a comparative fMRI study. J
605   Neurophysiol. 2009;101: 2581–2600. doi:10.1152/jn.91198.2008

606   32.   Racca A, Amadei E, Ligout S, Guo K, Meints K, Mills D. Discrimination of human and dog faces
607   and inversion responses in domestic dogs (Canis familiaris). Anim Cogn. 2010;13: 525–533.
608   doi:10.1007/s10071-009-0303-3

609   33.   Huber L, Racca A, Scaf B, Virányi Z, Range F. Discrimination of familiar human faces in dogs
610   (Canis familiaris). Learn Motiv. 2013;44: 258–269. doi:10.1016/J.LMOT.2013.04.005

611   34.   Albuquerque N, Guo K, Wilkinson A, Savalli C, Otta E, Mills D. Dogs recognize dog and human
612   emotions. Biol Lett. 2016;12: 20150883. doi:10.1098/rsbl.2015.0883

613 35. Huber L. How Dogs Perceive and Understand Us. Curr Dir Psychol Sci. 2016;25: 339–344.
614   doi:10.1177/0963721416656329

615 36. Maginnity ME, Grace RC. Visual perspective taking by dogs (Canis familiaris) in a Guesser–
616   Knower task: evidence for a canine theory of mind? Anim Cogn. 2014;17: 1375–1392.
617   doi:10.1007/s10071-014-0773-9

618 37. Catala A, Mang B, Wallis L, Huber L. Dogs demonstrate perspective taking based on
619   geometrical gaze following in a Guesser–Knower task. Anim Cogn. 2017;20: 581–589.
620   doi:10.1007/s10071-017-1082-x

621 38. Bunford N, Andics A, Kis A, Miklósi Á, Gácsi M. Canis familiaris As a Model for Non-Invasive
622   Comparative Neuroscience. Trends Neurosci. 2017;40: 438–452.
623   doi:10.1016/J.TINS.2017.05.003

624 39. Szabó D, Gábor A, Gácsi M, Faragó T, Kubinyi E, Miklósi Á, et al. On the Face of It: No
625   Differential Sensitivity to Internal Facial Features in the Dog Brain. Front Behav Neurosci.
626   2020;14. doi:10.3389/fnbeh.2020.00025

627 40. Dilks DD, Cook PF, Weiller SK, Berns HP, Spivak M, Berns GS. Awake fMRI reveals a
628   specialized region in dog temporal cortex for face processing. PeerJ. 2015; 3:e1115.
629   doi:10.7717/peerj.1115

630 41. Thompkins AM, Ramaiahgari B, Zhao S, Gotoor SSR, Waggoner P, Denney TS, et al.
631   Separate brain areas for processing human and dog faces as revealed by awake fMRI in dogs
632   (Canis familiaris). Learn Behav. 2018;46: 561–573. doi:10.3758/s13420-018-0352-z

633 42. Cuaya L V., Hernández-Pérez R, Concha L. Our faces in the dog's brain: Functional imaging
634   reveals temporal cortex activation during perception of human faces. PLoS One. 2016;11:
635   e0149431. doi:10.1371/journal.pone.0149431

636 43. Siniscalchi M, Lusito R, Vallortigara G, Quaranta A. Seeing Left- or Right-Asymmetric Tail
637   Wagging Produces Different Emotional Responses in Dogs. Curr Biol. 2013;23: 2279–2282.
638   doi:10.1016/J.CUB.2013.09.027

639 44. Duranton C, Range F, Virányi Z. Do pet dogs (Canis familiaris) follow ostensive and non-
640   ostensive human gaze to distant space and to objects? R Soc Open Sci. 2017;4: 170349.
641   doi:10.1098/rsos.170349

642 45. Topál J, Kis A, Oláh K. Dogs' Sensitivity to Human Ostensive Cues: A Unique Adaptation? The
643   Social Dog: Behavior and Cognition. Elsevier Inc.; 2014. pp. 319–346. doi:10.1016/B978-0-12-
644   407818-5.00011-5

645 46. Bräuer J, Kaminski J, Riedel J, Call J, Tomasello M. Making inferences about the location of
646   hidden food: Social dog, causal ape. J Comp Psychol. 2006;120: 38–47. doi:10.1037/0735-
647   7036.120.1.38

648 47. Fitch WT, Huber L, Bugnyar T. Social Cognition and the Evolution of Language: Constructing
649   Cognitive Phylogenies. Neuron. 2010;65: 795–814. doi:10.1016/J.NEURON.2010.03.011

650 48. Boch M, Karl S, Sladky R, Huber L, Lamm C, Wagner IC. Tailored haemodynamic response
651   function increases detection power of fMRI in awake dogs (Canis familiaris). Neuroimage.
652   2021;224: 117414. doi:10.1016/j.neuroimage.2020.117414

653 49. Karl S, Boch M, Virányi Z, Lamm C, Huber L. Training pet dogs for eye-tracking and awake
654   fMRI. Behav Res Methods. 2020;52. doi:10.3758/s13428-019-01281-7

655 50. Nitzsche B, Boltze J, Ludewig E, Flegel T, Schmidt MJ, Seeger J, et al. A stereotaxic breed-
656   averaged, symmetric T2w canine brain atlas including detailed morphological and volumetrical
657   data sets. Neuroimage. 2019;187: 93–103. doi:10.1016/j.neuroimage.2018.01.066

658 51. Czeibert K, Andics A, Petneházy Ö, Kubinyi E. A detailed canine brain label map for
659   neuroimaging analysis. Biol Futur. 2019;70: 112–120. doi:10.1556/019.70.2019.14

660 52. Shattuck DW, Mirza M, Adisetiyo V, Hojatkashani C, Salamon G, Narr KL, et al. Construction of
661   a 3D probabilistic atlas of human cortical structures. Neuroimage. 2008;39: 1064–1080.
662   doi:10.1016/j.neuroimage.2007.09.031

663 53. Fedorenko E, Hsieh P-J, Nieto-Castañón A, Whitfield-Gabrieli S, Kanwisher N. New method for
664   fMRI investigations of language: Defining ROIs functionally in individual subjects. J
665   Neurophysiol. 2010;104: 1177–1194. doi:10.1152/jn.00032.2010

666 54. Poldrack RA. Region of interest analysis for fMRI. Soc Cogn Affect Neurosci. 2007;2: 67–70.
667   doi:10.1093/scan/nsm006

668 55. Saxe R, Brett M, Kanwisher N. Divide and conquer: A defense of functional localizers.
669   Neuroimage. 2006;30: 1088–1096. doi:10.1016/J.NEUROIMAGE.2005.12.062

670 56. Julian JB, Fedorenko E, Webster J, Kanwisher N. An algorithmic method for functionally
671   defining regions of interest in the ventral visual pathway. Neuroimage. 2012;60: 2357–2364.
672   doi:10.1016/j.neuroimage.2012.02.055

673 57. Karl S, Boch M, Zamansky A, van der Linden D, Wagner IC, Völter CJ, et al. Exploring the
674   dog–human relationship by combining fMRI, eye-tracking and behavioural measures. Sci Rep.
675   2020;10: 22273. doi:10.1038/s41598-020-79247-5

676 58. Thompkins AM, Lazarowski L, Ramaiahgari B, Gotoor SSR, Waggoner P, Denney TS, et al.
677   Dog–human social relationship: representation of human face familiarity and emotions in the
678   dog brain. Anim Cogn. 2021;24: 251–266. doi:10.1007/s10071-021-01475-7

679 59. Cohen MA, Dilks DD, Koldewyn K, Weigelt S, Feather J, Kell AJE, et al. Representational
680   similarity precedes category selectivity in the developing ventral visual pathway. Neuroimage.
681   2019;197: 565–574. doi:10.1016/j.neuroimage.2019.05.010

682 60. Kriegeskorte N, Kievit RA. Representational geometry: integrating cognition, computation, and
683   the brain. Trends Cogn Sci. 2013;17: 401–412. doi:10.1016/J.TICS.2013.06.007

684 61. Kriegeskorte N, Mur M, Bandettini P. Representational similarity analysis - connecting the
685   branches of systems neuroscience. Front Syst Neurosci. 2008;2.
686   doi:10.3389/neuro.06.004.2008

687 62. Kriegeskorte N, Mur M, Ruff DA, Kiani R, Bodurka J, Esteky H, et al. Matching Categorical
688   Object Representations in Inferior Temporal Cortex of Man and Monkey. Neuron. 2008;60:
689   1126–1141. doi:10.1016/J.NEURON.2008.10.043

690 63. Rizzolatti G, Fogassi L, Gallese V. Neurophysiological mechanisms underlying the
691   understanding and imitation of action. Nat Rev Neurosci. 2001;2: 661–670.
692   doi:10.1038/35090060

693 64. Hamilton AF de C, Grafton ST. Goal Representation in Human Anterior Intraparietal Sulcus. J
694   Neurosci. 2006;26: 1133–1137. doi:10.1523/JNEUROSCI.4551-05.2006

695 65. Kilner JM, Neal A, Weiskopf N, Friston KJ, Frith CD. Evidence of Mirror Neurons in Human
696   Inferior Frontal Gyrus. J Neurosci. 2009;29: 10153–10159. doi:10.1523/JNEUROSCI.2668-

697   09.2009

698   66.   Törnqvist H, Somppi S, Kujala M V., Vainio O. Observing animals and humans: Dogs target
699   their gaze to the biological information in natural scenes. PeerJ. 2020;8: e10341.
700   doi:10.7717/peerj.10341

701   67.   Törnqvist H, Somppi S, Koskela A, Krause CM, Vainio O, Kujala M V. Comparison of dogs and
702   humans in visual scanning of social interaction. R Soc Open Sci. 2015;2: 150341.
703   doi:10.1098/rsos.150341

704   68.   Spriet C, Abassi E, Hochmann J-R, Papeo L. Visual object categorization in infancy. bioRxiv.
705   2021; 2021.02.25.432436. doi:10.1101/2021.02.25.432436

706   69.   Buttelmann D, Tomasello M. Can domestic dogs (Canis familiaris) use referential emotional
707   expressions to locate hidden food? Anim Cogn. 2013. doi:10.1007/s10071-012-0560-4

708   70.   Nagasawa M, Murai K, Mogi K, Kikusui T. Dogs can discriminate human smiling faces from
709   blank expressions. Anim Cogn. 2011;14: 525–533. doi:10.1007/s10071-011-0386-5

710   71.   Barber ALA, Randi D, Müller CA, Huber L. The Processing of Human Emotional Faces by Pet
711   and Lab Dogs: Evidence for Lateralization and Experience Effects. Guo K, editor. PLoS One.
712   2016;11: e0152393. doi:10.1371/journal.pone.0152393

713   72.   Racca A, Guo K, Meints K, Mills DS. Reading Faces: Differential Lateral Gaze Bias in
714   Processing Canine and Human Facial Expressions in Dogs and 4-Year-Old Children. PLoS
715   One. 2012;7: e36076. doi:10.1371/journal.pone.0036076

716   73.   Range F, Viranyi Z, Huber L. Selective Imitation in Domestic Dogs. Curr Biol. 2007;17: 868–
717   872. doi:10.1016/J.CUB.2007.04.026

718   74.   Soproni K, Miklósi Á, Topál J, Csányi V. Dogs' (Canis familiaris) Responsiveness to Human
719   Pointing Gestures. J Comp Psychol. 2002;116: 27–34. doi:10.1037//0735-7036.116.1.27

720   75.   Bray EE, Gnanadesikan GE, Horschler DJ, Levy KM, Kennedy BS, Famula TR, et al. Early-
721   emerging and highly heritable sensitivity to human communication in dogs. Curr Biol. 2021;31:
722   1–5. doi:10.1016/j.cub.2021.04.055

723   76.   Karl S, Sladky R, Lamm C, Huber L. Neural Responses of Pet Dogs Witnessing their
724   caregiver's Positive Interactions with a Conspecific: An fMRI Study. Cereb Cortex Commun.
725   2021;tgab047. doi:10.1093/TEXCOM/TGAB047

726   77.   Correia-Caeiro C, Guo K, Mills D. Bodily emotional expressions are a primary source of
727   information for dogs, but not for humans. Anim Cogn. 2021;1: 3. doi:10.1007/s10071-021-
728   01471-x

729   78.   Salomons H, Smith KCM, Callahan-Beckel M, Callahan M, Levy K, Kennedy BS, et al.
730   Cooperative Communication with Humans Evolved to Emerge Early in Domestic Dogs. Curr
731   Biol. 2021;31: 3137-3144.e11. doi:10.1016/J.CUB.2021.06.051

732   79.   Kaminski J. Domestic dogs: Born human whisperers. Curr Biol. 2021;31: R891–R893.
733   doi:10.1016/J.CUB.2021.05.063

734   80.   Siniscalchi M, D'Ingeo S, Minunno M, Quaranta A. Communication in Dogs. Animals. MDPI
735   AG; 2018. p. 131. doi:10.3390/ani8080131

736   81.   Long RA, Donovan TM, Mackay P, Zielinski WJ, Buzas JS. Effectiveness of Scat Detection
737   Dogs for Detecting Forest Carnivores. J Wildl Manage. 2007;71: 2007–2017.
738   doi:10.2193/2006-230

739   82.   Jamieson LTJ, Baxter GS, Murray PJ. Identifying suitable detection dogs. Applied Animal
740   Behaviour Science. Elsevier B.V.; 2017. pp. 1–7. doi:10.1016/j.applanim.2017.06.010

741   83.   Grimm-Seyfarth A, Harms W, Berger A. Detection dogs in nature conservation: A database on
742   their world-wide deployment with a review on breeds used and their performance compared to
743   other methods. Methods in Ecology and Evolution. British Ecological Society; 2021. pp. 568–
744   579. doi:10.1111/2041-210X.13560

745   84.   Dunn M, Degenhardt L. The use of drug detection dogs in Sydney, Australia. Drug Alcohol
746   Rev. 2009;28: 658–662. doi:10.1111/j.1465-3362.2009.00065.x

747   85.   Guest C, Otto CM. Editorial: Canine Olfactory Detection. Frontiers in Veterinary Science.
748   Frontiers Media S.A.; 2020. p. 100. doi:10.3389/fvets.2020.00100

749   86.   Berns GS, Brooks AM, Spivak M. Scent of the familiar: An fMRI study of canine brain
750   responses to familiar and unfamiliar human and dog odors. Behav Processes. 2015;110: 37–
751   46. doi:10.1016/J.BEPROC.2014.02.011

752   87.   Prichard A, Chhibber R, Athanassiades K, Spivak M, Berns GS. Fast neural learning in dogs: A
753   multimodal sensory fMRI study. Sci Rep. 2018;8: 14614. doi:10.1038/s41598-018-32990-2

754   88.   Jia H, Pustovyy OM, Wang Y, Waggoner P, Beyers RJ, Schumacher J, et al. Enhancement of
755   Odor-Induced Activity in the Canine Brain by Zinc Nanoparticles: A Functional MRI Study in
756   Fully Unrestrained Conscious Dogs. Chem Senses. 2016;41: 53–67.
757   doi:10.1093/chemse/bjv054

758   89.   Jia H, Pustovyy OM, Waggoner P, Beyers RJ, Schumacher J, Wildey C, et al. Functional MRI
759   of the Olfactory System in Conscious Dogs. Dhenain M, editor. PLoS One. 2014;9: e86362.
760   doi:10.1371/journal.pone.0086362

761   90.   Ramaihgari B, Pustovyy OM, Waggoner P, Beyers RJ, Wildey C, Morrison E, et al. Zinc
762   nanoparticles enhance brain connectivity in the canine olfactory network: Evidence from an
763   fMRI study in unrestrained awake dogs. Front Vet Sci. 2018;5: 127.
764   doi:10.3389/fvets.2018.00127

765   91.   Bräuer J, Blasi D. Dogs display owner-specific expectations based on olfaction. Sci Reports
766   2021 111. 2021;11: 1–10. doi:10.1038/s41598-021-82952-4

767   92.   Peirce JW. PsychoPy-Psychophysics software in Python. J Neurosci Methods. 2007;162: 8–
768   13. doi:10.1016/j.jneumeth.2006.11.017

769   93.   Wagner IC, van Buuren M, Bovy L, Fernández G. Parallel engagement of regions associated
770   with encoding and later retrieval forms durable memories. J Neurosci. 2016;36: 7985–7995.
771   doi:10.1523/JNEUROSCI.0830-16.2016

772   94.   R Core Team. R: A Language and Environment for Statistical Computing. Vienna, Austria: R
773   Foundation for Statistical Computing; 2020. Available: https://www.r-project.org/

774   95.   Yushkevich PA, Piven J, Hazlett HC, Smith RG, Ho S, Gee JC, et al. User-guided 3D active
775   contour segmentation of anatomical structures: Significantly improved efficiency and reliability.
776   Neuroimage. 2006;31: 1116–1128. doi:10.1016/J.NEUROIMAGE.2006.01.015

777   96.   Power JD, Barnes KA, Snyder AZ, Schlaggar BL, Petersen SE. Spurious but systematic
778   correlations in functional connectivity MRI networks arise from subject motion. Neuroimage.
779   2012;59: 2142–2154. doi:10.1016/J.NEUROIMAGE.2011.10.018

780   97.   Power JD, Mitra A, Laumann TO, Snyder AZ, Schlaggar BL, Petersen SE. Methods to detect,

781   characterize, and remove motion artifact in resting state fMRI. Neuroimage. 2014;84: 320–341.

782   doi:10.1016/j.neuroimage.2013.08.048

783 98. Mumford JA, Turner BO, Ashby FG, Poldrack RA. Deconvolving BOLD activation in event-

784   related designs for multivoxel pattern classification analyses. Neuroimage. 2012;59: 2636–

785   2643. doi:10.1016/j.neuroimage.2011.08.076

786 99. Kriegeskorte N, Goebel R, Bandettini P. Information-based functional brain mapping. Proc Natl

787   Acad Sci U S A. 2006;103: 3863–3868. doi:10.1073/pnas.0600244103

788 100. Nichols TE, Holmes AP. Non-parametric procedures. Statistical Parametric Mapping: The

789   analysis of Functional Brain Images. Amsterdam: Elsevier; 2007. pp. 253–272.

790 101. Wickham H. ggplot2: Elegant Graphics for Data Analysis. Springer-Verlag New York; 2016.

791   Available: https://ggplot2.tidyverse.org

792 102. Allen M, Poggiali D, Whitaker K, Marshall TR, Kievit RA. Raincloud plots: A multi-platform tool

793   for robust data visualization [version 1; peer review: 2 approved]. Wellcome Open Res. 2019;4.

794   doi:10.12688/wellcomeopenres.15191.1

795

796

9 Supporting information

9.1 Stimulus material: luminance and spatial extent

Luminance was set to 100 for all images and background, grid-scrambled images were created based on images equally drawn from each category to control for potential low-level visual differences. Face and body images vary in spatial extent (= ratio image / background) due to their shape (mean values: faces = 58.53; bodies = 29.42; $t(118) = 21.17$, $p < 0.0001$), matching them in spatial extent would have required resizing the face images to half their size resulting in less ecologically valid images, but we matched dog and human images within the body and face categories (mean values faces: dogs = 58.55; humans = 58.50; $t(58) = 0.03$, $p = 0.98$; means bodies: dogs = 30.97; humans = 27.87; $t(58) = 1.33$, $p = 0.19$). Further, half of the object images were matched in spatial extent to either body (mean values: bodies = 29.42, matched objects = 29.86, $t(73) = -0.17$, $p = 0.86$) or face (mean values: faces = 58.53, matched objects = 57.23, $t(73) = 0.78$, $p = 0.44$) images and scrambled images were created based on images equally drawn from each category.

9.2 Anatomical search spaces

We localized face and body areas in restrained search spaces to also retrieve anatomically more precise information. For the dog participants, we could not build on previous research due to different template spaces or data unavailability and therefore selected all task-responsive gyri as search spaces. We determined them performing a group-level activation comparison entering the visual stimulation contrast (all conditions > implicit visual baseline) from the first task run in a second-level one sample *t*-test. Since the majority of significant clusters expanded across more than one anatomical region, we decided to not only select regions with a significant local maxima (**Table S1**, section "dog participants**", Fig 1C**) but all gyri with visual responsive voxels. This resulted in six search spaces for potential face or body regions: medial

823   suprasylvian, caudal suprasylvian, ectomarginal, occipital, marginal and splenial gyrus

824   (**Fig 2A**). For the human participants, we used bilateral fusiform and occipital face area

825   parcels as face area search spaces and bilateral fusiform and extrastriate body area

826   parcels as body area search spaces derived from previous research [56]. Selecting the

827   top-10% voxels resulted in the following functional region of interest (fROI) sizes for

828   each hemisphere: medial suprasylvian gyrus (32 voxels), caudal suprasylvian gyrus

829   (27 voxels), marginal gyrus (35 voxels; for one dog 23 voxels in the left hemisphere

830   due to lower number of active voxels in contrast bodies > inanimate objects),

831   ectomarginal gyrus (31 voxels), splenial gyrus (34 voxels) and occipital gyrus (23

832   voxels). For the human participants, selecting the top-10% voxels from each of the four

833   parcels [56] resulted in the following fROI sizes: extrastriate body area (each

834   hemisphere: 137 voxels), fusiform body area (left: 53 voxels; right: 102 voxels),

835   occipital face area (left: 21 voxels, except one participant only had 15 active voxels,

836   and another had no active voxels; right: 79 voxels), fusiform face area (left: 216 voxels,

837   right: 241 voxels).

9.3 Supplemental figures
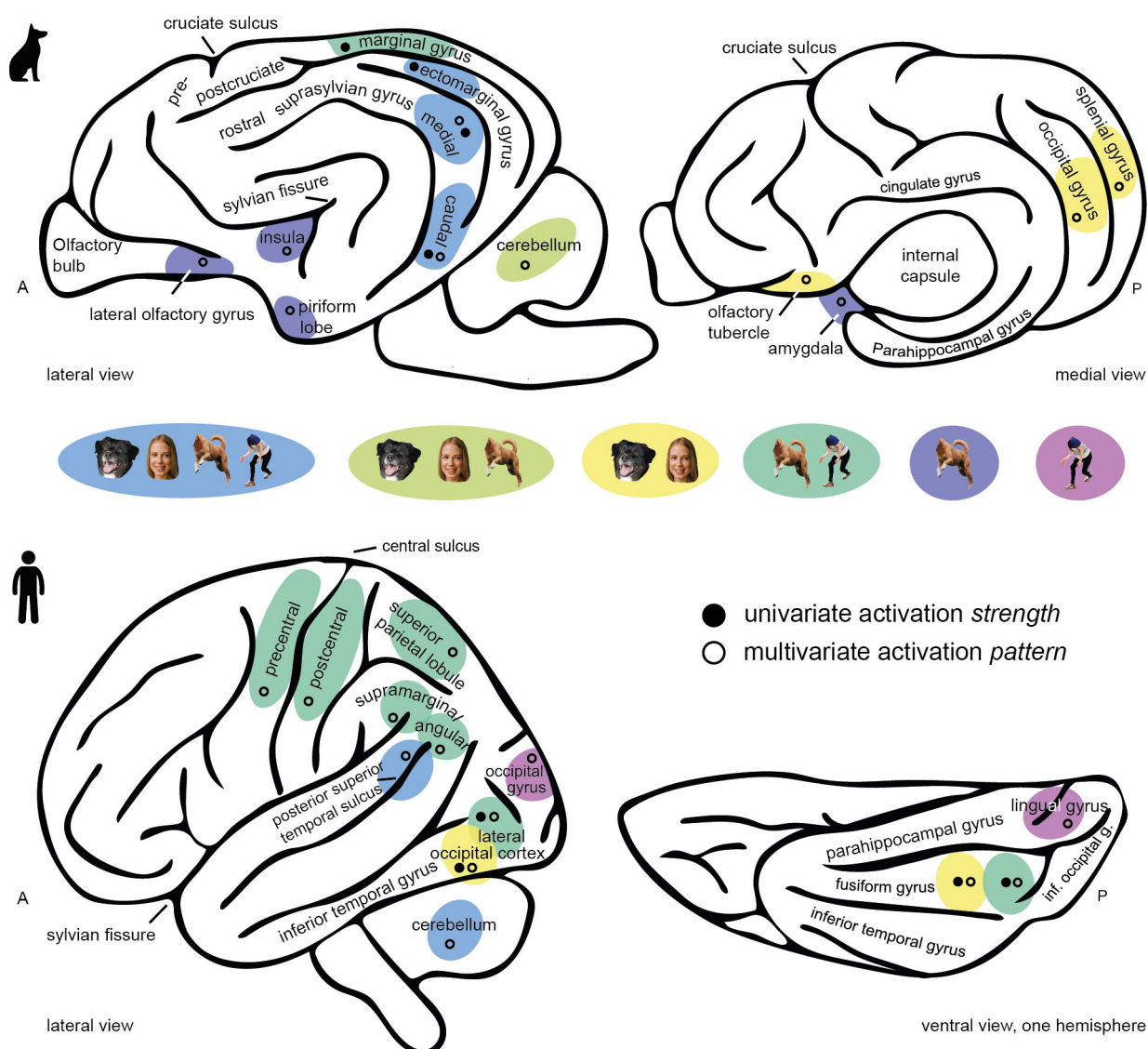
**Fig S1.** *Summary of the main study findings*. Results from the functional regions of interest (univariate activation strength) and representational similarity analysis (multivariate activation pattern) illustrating the results on schematic brain figures. For simplification, observed results are always summarized on one hemisphere; they do not mark the exact but the approximate anatomical location.
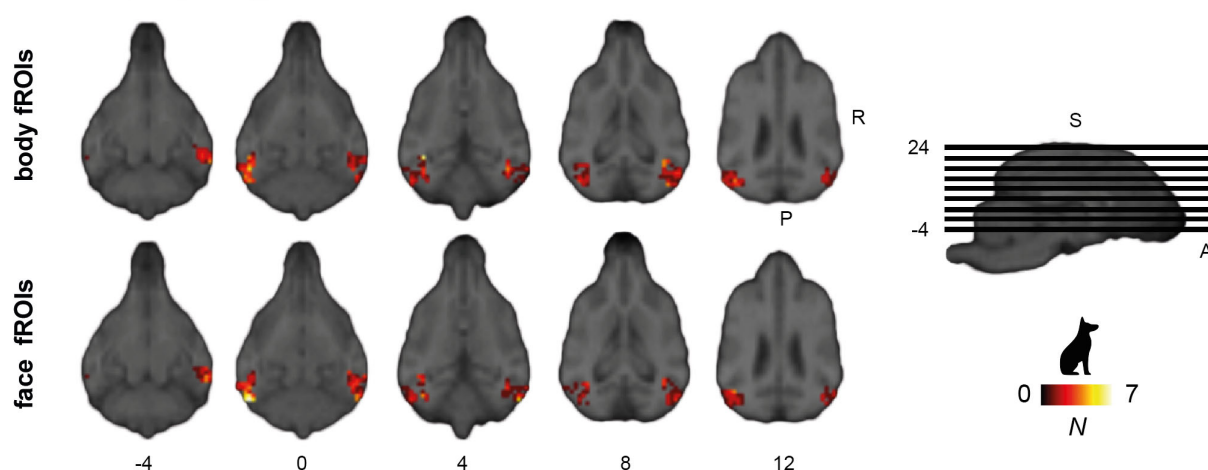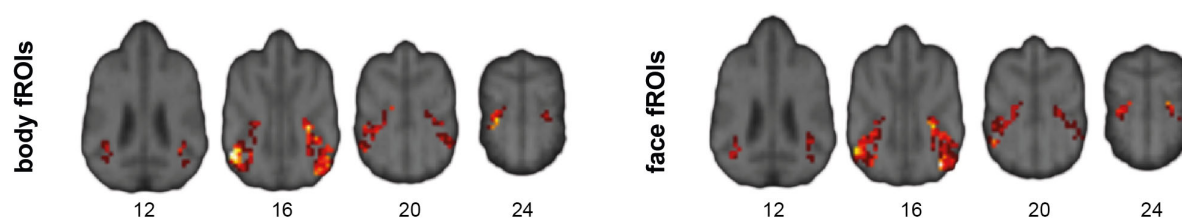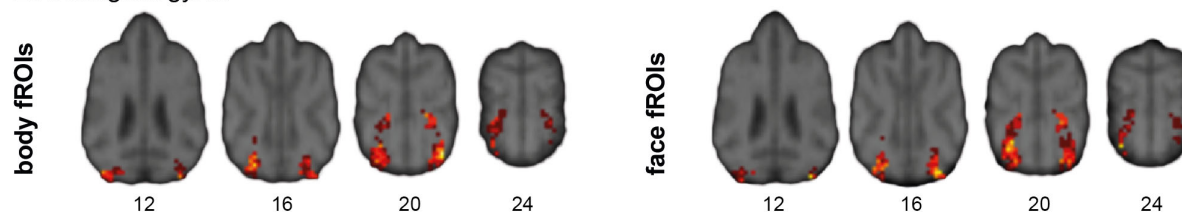
Fig S2. *Overlap of individual functional regions-of-interest (fROIs) from dog participants.* Individual fROIs were defined for faces (> inanimate objects) and bodies (> inanimate objects) within multiple anatomical search spaces (A-D) based on the data from localizer data set (i.e., first task run). The colour of the heat map indicates the amount of overlap between the fROIs of all dog participants. We observed slight individual differences in anatomical location between participants as indicated by a maximum overlap of $N = 7$ from overall 15 participants. The axial plane in panel A (top row) shows the anatomical locations posterior (P) and right hemisphere (R); all axial planes displayed have the same orientation. The sagittal plane displays the cut coordinates (z) and the anatomical locations superior (S) and anterior (A); z-coordinates refer to a canine-breed averaged template [50].

841
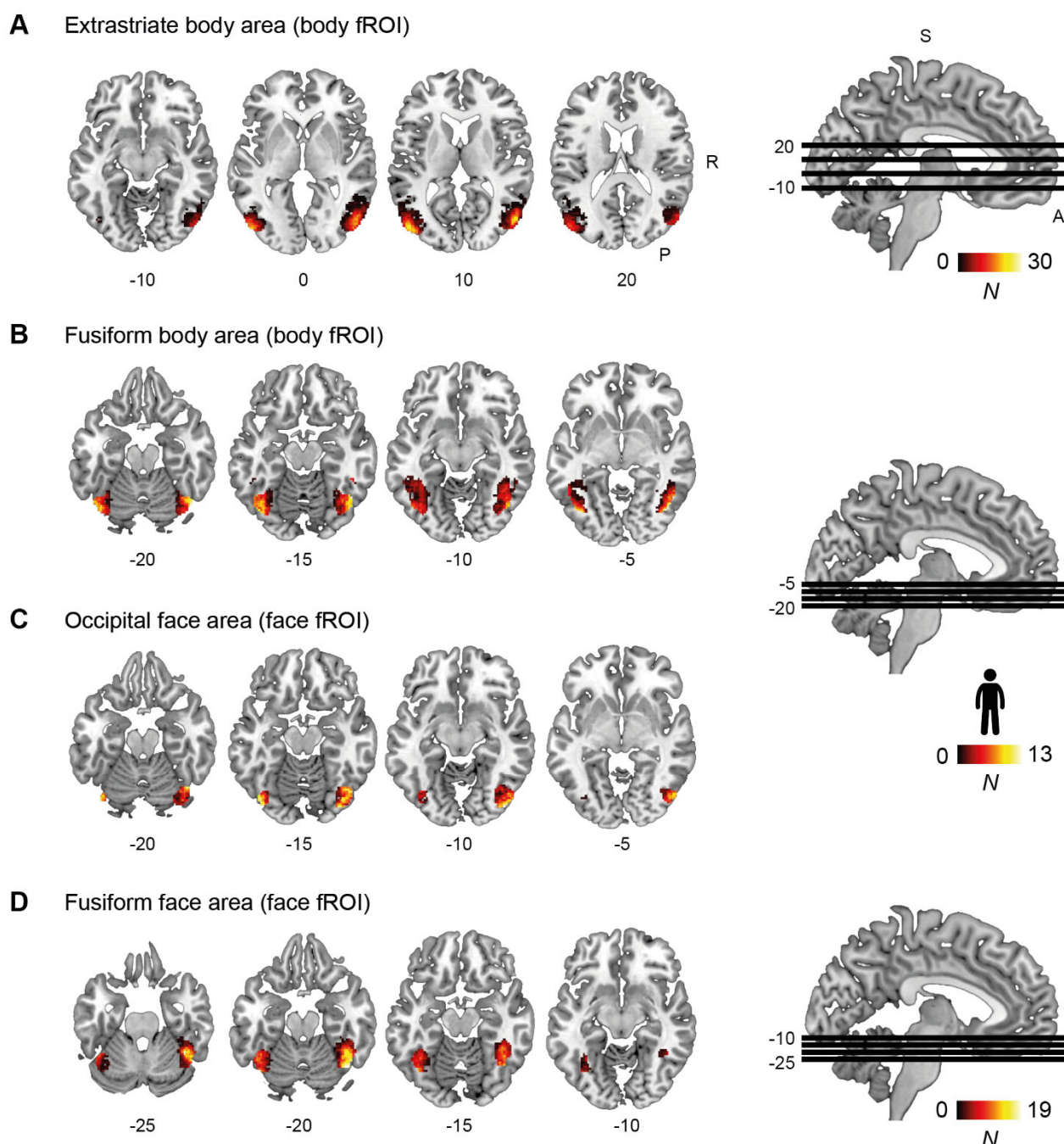
Fig S3. *Overlap of individual functional regions-of-interest (fROIs) from human participants.* Individual fROIs were defined for faces (> inanimate objects) and bodies (> inanimate objects) within multiple anatomical search spaces (A-D) based on the data from the localizer data set (i.e. first task run). The colour of the heat map indicates the amount of overlap between the fROIs of all humans. We observed slight individual differences in anatomical location between participants as indicated by a maximum overlap of N = 30 from overall 40 participants. The axial plane in panel A shows the anatomical locations posterior (P) and right hemisphere (R); all axial planes displayed have the same orientation. The sagittal planes display the cut coordinates (z) and the anatomical locations superior (S) and anterior.

842

843   ## 9.4 Supplemental tables

Table S1. Task-related activation: localizer data set (task run 1)

Contrast & brain region	Coordinates			z-value	cluster size
	x	y	z		
All conditions > implicit visual baseline					
Dog participants					
L medial suprasylvian gyrus	-16	-23	15	4.56	16
L caudal suprasylvian gyrus	-22	-26	-1	4.39	17
L medial suprasylvian gyrus	17	-26	16	4.32	74
L ectomarginal gyrus	-9	-27	21	4.29	52
R ectomarginal gyrus	10	-29	21	4.12	37
R caudal suprasylvian gyrus	22	-24	-1	4.04	24
Human participants					
R middle occipital gyrus	48	-70	-8	Inf	13423
R middle frontal gyrus	20	30	0	Inf	248
L hippocampus	-20	-30	-4	Inf	252
L inferior temporal gyrus	-28	-4	-36	6.89	65
R cerebellum	22	-42	-44	6.80	45

Effects were tested for significance with a cluster defining threshold of $p < .001$ and a cluster probability threshold of $p < 0.05$ FWE corrected for multiple comparisons for the dog data and a whole-brain FWE correction for the human data. We report the first local maximum within each cluster for both one sample *t*-tests and for the human data we limit the list to the first five cluster with the highest peak *z*-values. Coordinates for the dog data represent the location of the peak voxels referring to the canine breed-averaged template space[50]; the template along with another dog atlas[51] served to determine anatomical nomenclature for the dog data. Human data coordinates refer to the stereotactic Montreal Neurological Institute (MNI) space we obtained anatomical nomenclature from the Laboratory for Neuro Imaging (LONI) Brain Atlas[52] (LBPA40, http://www.loni.usc.edu/atlases/). Data of both samples is also presented in **Fig 1C**. L, left; R, right.

844

Table S2. Results from one-way[a] repeated measures analyses of variance (ANOVAs)

Search space (predictor: image category)	df_{Num}	df_{Den}	F	p	η^2_g
Dog participants					
Individual body fROIs defined based on bodies > inanimate objects contrast from run 1					
Medial suprasylvian gyrus	2.26	31.68	26.01	**< .0001**	.37
Caudal suprasylvian gyrus	2.26	31.66	12.53	**< .0001**	.25
Ectomarginal gyrus	1.87	26.23	7.48	**.003**	.13
Marginal gyrus	2.36	33.08	8.69	**.001**	.17
Splenial gyrus	2.66	37.19	1.69	.191	.07
Occipital gyrus	2.26	31.58	0.74	.499	.02
Individual face fROIs defined based on faces > inanimate objects contrast from run 1					
Medial suprasylvian gyrus	2.05	28.77	22.13	**< .0001**	.30
Caudal suprasylvian gyrus	2.49	34.90	17.34	**< .0001**	.30
Ectomarginal gyrus	1.75	24.55	12.11	**< .0001**	.18
Marginal gyrus	1.95	27.30	6.38	**.006**	.12
Splenial gyrus	2.34	32.72	1.61	.214	.06
Occipital gyrus	2.26	31.58	0.74	.499	.02
Human participants					
Individual body fROIs defined based on bodies > inanimate objects contrast from run 1					
Extrastriate body area	1.73	67.49	227.01	**< .0001**	.71
Fusiform body area	2.00	77.98	152.22	**< .0001**	.59
Individual face fROIs defined based on faces > inanimate objects contrast from run 1					
Occipital face area	1.98	77.04	175.25	**< .0001**	.64
Fusiform face area	2.12	82.86	187.29	**< .0001**	.63

Note. [a]Dependent variable: *image category* (levels: bodies, faces, inanimate objects, scrambled). *P*-values for group comparison investigating the same research question (i.e., species sensitivity for bodies, species sensitivity for bodies) are Bonferroni-adjusted, resulting in an adjusted *p*-value of 0.008 (= 0.05/6) for the dog body functional regions of interest (fROIs) and face fROIs respectively and an adjusted *p*-value of 0.025 (= 0.05/2) for the human face and body fROIs. *P*-values surviving the adjusted threshold are in bold. Post-hoc comparison results are presented in **Fig 2B**. df_{Num}, degrees of freedom numerator; df_{Den} degrees of freedom denominator; η^2_g, generalized eta-squared.

845

Table S3. Results from 2 × 2[a] repeated measures analyses of variance (ANOVAs)

Search space, predictor	df_{Num}	df_{Den}	F	p	η^2_g
Dog participants					
Individual body fROIs defined based on bodies > inanimate objects contrast from run 1					
Medial suprasylvian gyrus					
Species	1	14	3.54	.081	.02
Image category	1	14	7.26	.017	.03
Species × image category	1	14	2.18	.167	.02
Caudal suprasylvian gyrus					
Species	1	14	3.75	.073	.02
Image category	1	14	0.206	.174	.01
Species × image category	1	14	.01	.926	.00
Ectomarginal gyrus					
Species	1	14	2.57	.131	.01
Image category	1	14	1.42	.253	.01
Species × image category	1	14	4.57	.051	.02
Marginal gyrus					
Species	1	14	0.50	.493	.00
Image category	1	14	7.90	.014	.05
Species × image category	1	14	2.25	.156	.03
Splenial gyrus					
Species	1	14	0.03	.859	.00
Image category	1	14	3.71	.074	.03
Species × image category	1	14	1.26	.281	.02
Occipital gyrus					
Species	1	14	1.10	.312	.01
Image category	1	14	0.01	.921	.00
Species × image category	1	14	0.26	.620	.00
Individual face fROIs defined based on faces > inanimate objects contrast from run 1					
Medial suprasylvian gyrus					
Species	1	14	2.51	.135	.01
Image category	1	14	7.11	.018	.03
Species × image category	1	14	1.95	.185	.02
Caudal suprasylvian gyrus					
Species	1	14	1.61	.225	.02
Image category	1	14	10.20	.007	.06
Species × image category	1	14	0.03	.857	.00
Ectomarginal gyrus					
Species	1	14	2.75	.120	.02
Image category	1	14	1.86	.194	.01
Species × image category	1	14	4.22	.059	.03
Marginal gyrus					

Species	1	14	0.08	.786	.00
Image category	1	14	10.03	.007	.07
Species × image category	1	14	1.23	.286	.01
Splenial gyrus					
Species	1	14	0.26	.617	.00
Image category	1	14	1.73	.209	.02
Species × image category	1	14	.70	.416	.01
Occipital gyrus					
Species	1	14	1.21	.289	.02
Image category	1	14	0.03	.855	.00
Species × image category	1	14	3.90	.068	.02
Human participants					
Individual body fROIs defined based on bodies > inanimate objects contrast from run 1					
Extrastriate body area					
Species	1	39	3.15	.084	.01
Image category	1	39	187.26	**< .0001**	.39
Species × image category	1	39	14.15	**.001**	.02
Fusiform body area					
Species	1	39	0.54	.469	.00
Image category	1	39	15.24	**< .0001**	.04
Species × image category	1	39	1.43	.239	.00
Individual face fROIs defined based on faces > inanimate objects contrast from run 1					
Occipital face area					
Species	1	39	0.02	.889	.00
Image category	1	39	36.99	**< .0001**	.07
Species × image category	1	39	1.14	.292	.00
Fusiform face area					
Species	1	39	12.24	**.001**	.02
Image category	1	39	45.23	**< .0001**	.11
Species × image category	1	39	0.28	.600	.00

Note. [a]Dependent variables are *species* (levels: dog, human) and *image category* (levels: bodies, faces). *P*-values for group comparison investigating the same research question (i.e., category selectivity for bodies, category selectivity for faces) are Bonferroni-adjusted, resulting in an adjusted *p*-value of 0.008 (= 0.05/6) for the dog body functional regions of interest (fROIs) and face fROIs respectively and an adjusted *p*-value of 0.025 (= 0.05/2) for the human face and body fROIs. *P*-values surviving the adjusted threshold are in bold, for the dog data none of the *p*-values survived the adjusted threshold. df_{Num}, degrees of freedom numerator; df_{Den} degrees of freedom denominator; η^2_g, generalized eta-squared.

846

Table S4. Dog data: Pattern similarity during face, body and object perception

Contrast & brain region	Coordinates (breed-averaged template)			*t*-value	cluster size
	x	y	z		
Bodies [dog bodies × human bodies] > inanimate objects					
R caudal suprasylvian gyrus	19	-24	4	5.77	116
Faces [dog faces × human faces] > inanimate objects					
R marginal gyrus	5	-35	21	7.01	245
R olfactory tuberculum	8	8	-2	6.16	80
Conspecific (dog) bodies > heterospecific (human) bodies					
L caudal suprasylvian gyrus	-16	-27	4	5.21	99
L piriform lobe	-15	-3	-4	5.18	95
Animate [dog bodies × human bodies × dog faces × human faces] > inanimate stimuli					
R splenial gyrus	5	-32	7	5.38	70
R caudal suprasylvian gyrus	19	-24	3	5.25	72

Effects were tested for significance with a cluster defining threshold of *p* <.005 and a cluster probability threshold of *p* < 0.05 FWE corrected for multiple comparisons. We report the first local maximum within each cluster for all paired sample *t*-tests. The results from the paired sample *t*-tests comparing faces [dog faces × human faces] vs. bodies [dog bodies × human bodies] and conspecific (dog) faces vs. heterospecific (human) faces along with the reversed contrasts [dog bodies × human bodies] < inanimate objects, [dog faces × human faces] < inanimate objects, conspecific (dog) bodies < heterospecific (human) bodies and [dog bodies × human bodies × dog faces × human faces] < inanimate objects did not survive the statistical threshold. Coordinates represent the location of the peak voxels referring to the canine breed-averaged template space[50]; the template along with another dog atlas[51] served to determine anatomical nomenclature for the dog data. Data is also presented in **Fig 3B-D**. L, left; R, right.

847

Table S5. Human data: Pattern similarity during face, body and object perception

Contrast & brain region	Coordinates (MNI space)			t-value	cluster size
	x	y	z		
Bodies [dog bodies × human bodies] > inanimate objects					
R middle occipital gyrus	56	-72	6	14.98	14018
L middle occipital gyrus	-54	-78	10	12.32	1622
L cerebellum	-4	-70	-40	7.33	585
L superior parietal gyrus	-26	-62	68	6.65	1383
R superior frontal gyrus	6	62	-4	6.17	881
L precentral gyrus	-26	-10	50	5.26	570
Bodies [dog bodies × human bodies] < inanimate objects					
L inferior temporal gyrus	-22	-48	-12	11.26	6678
Faces [dog faces × human faces] > inanimate objects					
R fusiform gyrus	46	-42	-20	9.35	1088
Faces [dog faces × human faces] < inanimate objects					
L cerebellum	-20	-54	-18	14.20	7002
R lingual gyrus	24	-56	-8	11.84	5198
L precentral gyrus	-46	6	32	4.77	353
Faces [dog faces × human faces] > bodies [dog bodies × human bodies]					
R lingual gyrus	6	-88	0	11.35	3461
Faces [dog faces × human faces] < bodies [dog bodies × human bodies]					
R middle occipital gyrus	34	-72	10	14.21	39057
R middle orbitofrontal gyrus	24	42	-14	5.53	1087
R cerebellum	8	-72	-38	5.19	572
R cingulate gyrus	2	6	26	4.76	267
Conspecific (human) bodies > heterospecific (dog) bodies					
R fusiform gyrus	44	-44	-22	5.76	1053
L middle occipital gyrus	-54	-72	12	4.87	267
R middle temporal gyrus	40	-54	12	4.81	468
R superior parietal gyrus	16	-54	42	4.60	466
Heterospecific (dog) faces > conspecific (human) faces					
L middle occipital gyrus	-16	-94	6	7.20	8147
Brainstem	6	-40	-26	4.64	618
R middle occipital gyrus	56	-72	0	5.71	349
Animate [dog bodies × human bodies × dog faces × human faces] > inanimate objects					

R middle occipital gyrus	56	-72	0	9.09	2035
L cerebellum	-4	-70	-42	7.30	277
R postcentral gyrus	36	-26	48	5.09	403
R superior parietal gyrus	38	-44	68	4.82	338
R superior frontal gyrus	8	52	-8	4.77	564
Animate [dog bodies × human bodies × dog faces × human faces] < inanimate objects					
L cerebellum	-22	-50	-18	12.63	11878

Effects were tested for significance with a cluster defining threshold of *p* <.001 and a cluster probability threshold of *p* < 0.05 FWE corrected for multiple comparisons. We report the first local maximum within each cluster for all paired sample *t*-tests. Results from the reversed contrasts conspecific (human) bodies < heterospecific (dog) bodies and heterospecific (dog) faces < conspecific (human) did not survive the statistical threshold. Coordinates refer to the stereotactic Montreal Neurological Institute (MNI) space and represent the location of the peak voxels. We obtained anatomical nomenclature from the Laboratory for Neuro Imaging (LONI) Brain Atlas [52] (LBPA40, http://www.loni.usc.edu/atlases/). Data is also presented in **Fig 3B-D**.

848